CHALMERS
UNIVERSITY OF TECHNOLOGY

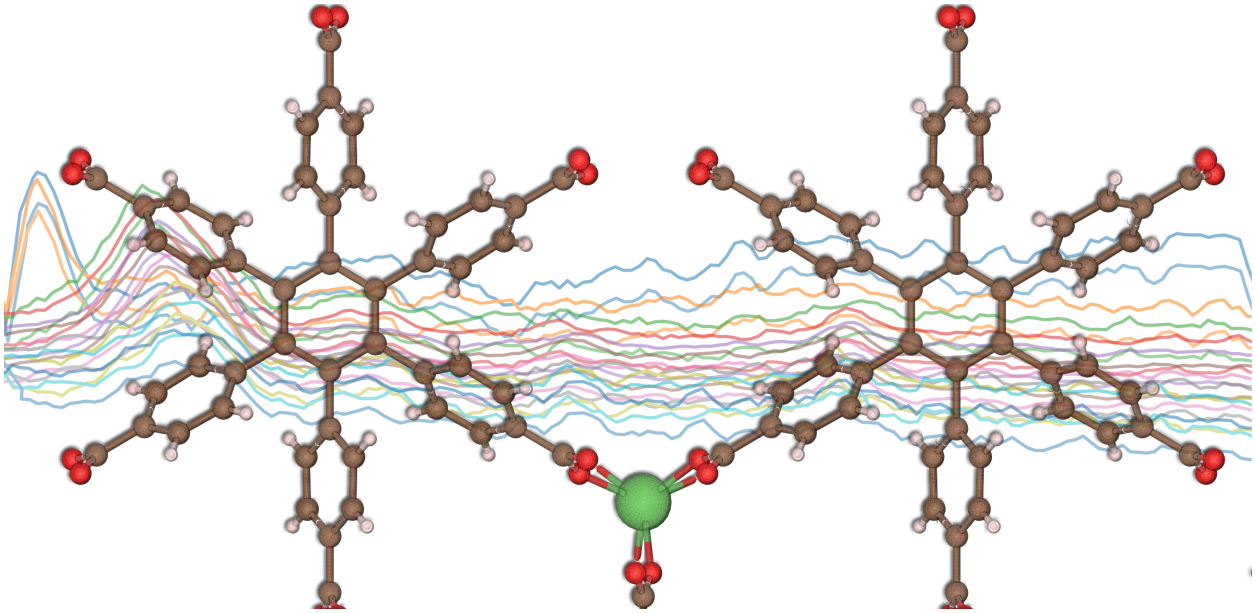

Local structure and dynamics of two novel metal-organic framework materials investigated with Raman spectroscopy and neutron scattering techniques

Master's thesis in Nanotechnology

David Reinsfelt

DEPARTMENT OF CHEMISTRY AND CHEMICAL ENGINEERING
CHALMERS UNIVERSITY OF TECHNOLOGY
Gothenburg, Sweden 2024
www.chalmers.se

Master's thesis 2024

Local structure and dynamics of two novel metal-organic framework materials investigated with Raman spectroscopy and neutron scattering techniques

David Reinsfelt

CHALMERS
UNIVERSITY OF TECHNOLOGY

Department of Chemistry and Chemical Engineering
Division of Energy and Materials
Chalmers University of Technology
Gothenburg, Sweden 2024

Local structure and dynamics of two novel metal-organic framework materials investigated with Raman spectroscopy and neutron scattering techniques
DAVID REINSFELT

© David Reinsfelt, 2024.

Examiner: Daniel Weber, Assistant Professor, Division of Energy and Materials, Department of Chemistry and Chemical Engineering
Supervisor: Maths Karlsson, Full Professor, Division of Energy and Materials, Department of Chemistry and Chemical Engineering

Master's Thesis 2024
Department of Chemistry and Chemical Engineering
Division of Energy and Materials
Chalmers University of Technology
SE-412 96 Gothenburg
Telephone +46 31 772 1000

Cover: The structure of the metal-organic framework material called CTH-17 with examples of Raman spectra in the background.

Gothenburg, Sweden 2024

Local structure and dynamics of two novel metal-organic framework materials investigated with Raman spectroscopy and neutron scattering techniques

DAVID REINSFELT
Department of Chemistry and Chemical Engeering
Chalmers University of Technology

Abstract

Metal-Organic Frameworks (MOFs) show a wide variety of new applications in areas such as energy storage, catalysis, sensor technology and drug delivery, due to their inherent porous structures and facile tunability. Some MOFs also show structural flexibility upon temperature variation, which opens up even more possibilities for applications. However, the local structure and dynamics, underpinning this flexibility, are often unclear. This thesis deals with a study of the local structure and dynamics of two newly discovered MOFs, namely La_2(CPB) and Ce_2(CPB), where CPB refers to the hexagon shaped hexatopic linker 1,2,3,4,5,6-hexakis(4- carboxyphenyl)benzene. La_2(CPB), also called CTH-17, has previously proven to show gate opening effects under CO_2 gas sorption measurements by drastically increase the adsorption after certain pressure values. Changes in the crystal structure in the form of twisted phenyl rings and stretching in the rod direction of the rod-shaped CTH-17 have also been observed when measured with SCXRD in 90 K, 300 K and 500 K. This study seeks to confirm these observed structure changes by studying local atomic vibrations, using Raman spectroscopy and inelastic neutron scattering (INS). The goal is not only to observe the static material structures before and after undergone the mentioned changes observed with SCXRD measurements, but also to observe the structural dynamics upon temperature variation.

The samples were synthesized with a solvothermal synthesis method which yielded La_2(CPB) and Ce_2(CPB) as the majority phase with variable amounts of La or Ce-formate as side phases. Both Raman and INS spectra of La_2(CPB) and Ce_2(CPB) show negligible differences, indicating that their local structure and dynamics are very similar. Room temperature Raman spectroscopy measurements of activated La_2(CPB) and Ce_2(CPB) samples show photoluminescence. The variable temperature Raman spectroscopy results show indications of DMF leaving the porous structures around 200-300 °C. Linearly shifting frequency trends with increased temperature is observed for several bands indicating thermal expansion, and a big irreversible shift at 300 °C is observed indicating a new structural phase. Indications of luminescence in combination with DMF leaving the structure is also observed.

The similarities between La_2(CPB) and Ce_2(CPB) suggests that changing the metal ion nodes in this type of hexagonal shaped MOF from La to a similar metal such as Ce, does not alter the local structure and dynamics. The supposed observed thermal expansion and structural phase shift for both La_2(CPB) and Ce_2(CPB) could explain the gate opening effect during CO_2 gas sorption measurements by showing that the porous structure changes upon increased temperature which can create more space for molecules to enter the pores.

Acknowledgements

I would like to thank Maths Karlsson for giving me the opportunity to do this project and for assisting me throughout the entire process.

I would also like to thank Rasmus Lavén for assisting me and providing me with expertise knowledge in the field with excellent explanations and discussions.

And thank you Anna Martinelli for helping me with Raman spectroscopy expertise, Danaé Morel, William Reinholdsson and Lars Öhrström for assisting me through the synthesis and chemistry parts, Elena Naumovska and Vicent Ssenteza for helping me with SEM measurements, Jeff Armstrong for helping me with INS measurements, and Pedram Pakmehr for great discussions and for sharing your knowledge in the field.

Finally a big thank you to everyone at the department for being so helpful, kind and positive towards me and the people around you. It really has been nice to go to the office these six months.

List of Acronyms

CIF	Crystallographic Information File
CPB	1,2,3,4,5,6-hexakis(4- carboxyphenyl)benzen
DABCO	1,4-diazabicyclo[2.2.2]octane
DMF	Dimethylformamide
DUT	Dresden University of Technology
INS	Inelastic Neutron Scattering
MOF	Metal-Organic Framework
NDC	Naphthalen Dicarboxylic
PXRD	Powder X-Ray Diffraction
QENS	Quasi Elastic Neutron Scattering
SCXRD	Single Crystal X-Ray Diffraction
SEM	Scanning Electron Microscope
ZIF	zeolite imidazolate frameworks

Contents

List of Figures

List of Tables

1
Introduction

This thesis presents an analysis of the local structure and dynamics of metal-organic frameworks (MOFs). MOFs belong to a class of porous materials. The porosity makes them suitable to do chemistry inside the pores. The pores can be filled with molecules, their large surface area makes them efficient absorbers of molecules, they can be used for homogeneous catalysis, and they can be pumped up and increase in volume by inflating them with gas. In effect, they show potential for application in diverse technologies such as in energy storage, catalysis, and gas separation [1][2][3][4][5]. They are also predicted to replace some traditionally used functional materials such as zeolites and microporous carbons, as a more easy to tune and more reusable option [1].

Many MOFs have also shown to be "soft" and posses different forms of structural flexibility when subject to external stimuli, giving them additional properties. This has opened up a new field within MOF studies where properties such as selective adsorption and desorption is investigated, with the potential to be applied in for instance selective gas storage or drug delivery technologies. There are MOFs showing so called breathing effects, where the molecular network folds itself and the metal nodes in the framework act as axles [6]. Others show gate opening effects, where the porosity suddenly gets accessible for guest molecules after a certain threshold of external stimuli. Swelling effects is an example of that where the MOF unit cell volume increases without changing in unit cell chape or space group [7]. There are several more types of structural flexibilities in MOFs, and typically they show gate opening effects when gas sorption measurements are made on them. This thesis focus on a type of flexibility called linker rotation, which causes a gate-opening effect by twisting the organic part of the framework (linker), and in that way opening the pores, making it easier for guest molecules to enter [8]. However, the nature of the local structure and dynamics to this twisting effect and how it translates into a flexibility of the entire structure is not fully understood.

The goal of this study is to make a contributional step in this understanding, and to try to observe the dynamical changes that occurs in the materials when subject to external stimuli, in this case temperature change. This knowledge could aid in the future development for flexible MOF designs with tailored properties.

1.1 Scientific background

In 2022 F.M. Amombo, L. Öhrström et al., reported indications of gate-opening effects in a MOF called CTH-17, consisting of lanthanum(III) and the propeller-like linking organic molecule named 1,2,3,4,5,6-hexakis(4-carboxyphenyl)- benzene (CPB) [9]. Carbon dioxide sorption showed that at pressures of 0.45 mmol/g, which is approximately 1 molecule per unit cell, the sorption starts to increase rapidly, indicating flexibility or a gate opening behavior. The suggested explanation to this behavior was that the 6 phenyl-rings of the propeller-like structure of the CPB linker undergoe rotation to "open up" the structure for guest molecules to enter. Single-crystal X-ray diffraction (SCXRD) measurements at 90 K, 300 K, and 500 K showed structural differences that indicated rotations of the phenyl groups, and possibly stretching along the rod axis of the structure, see Figure 1.1. In 300 K a structure belonging to the space group $P622$ (a chiral space group) could be assigned, and in 500 K both space group $P622$ and P/mmm could be assigned. Density-functional theory (DFT) calculations were made to get further understanding of the dynamics of the structure changes. DFT calculated models could be assigned to both space group $P622$ and $P6/mmm$, where the former structure was the global energy minimum and the latter a local energy minimum. It was shown that in order for the structure to change between these space groups, a rotation of the phenyl rings, and streching along the rod-axis was needed. The phenyl rings in the linkers need more room to twist, therefore the linkers are separated by stretching of the rod. With these strong indications of dynamics in the material, researchers at Chalmers measured the dynamics of CTH-17 using the technique quasielastic neutron scattering (QENS). Preliminary results from these measurements show presence of rotational activity of the phenyl rings. However, they were not able to conclude the origin of the vibrations, and the signatures of twisting of phenyl rings. Further investigations regarding the vibrational dynamics of the phenyl rings, and the surrounding molecular structure is needed. Especially in relation to variable temperature, in the temperature ranges 90 K to 500 K where the structure supposedly undergoes changes.

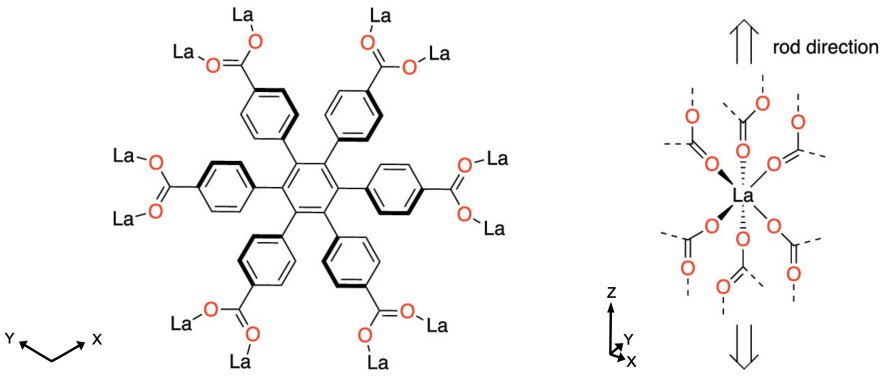

Figure 1.1: Left figure shows CTH-17 with the CPB-linker centered (the six phenyl rings connected to the central benzene ring). Right image shows the stacking behavior of the structure forming a rod-shaped MOF. The image is adapted with permission from ref. [9], Copyright (2022) American Chemical Society.

1.2 Aim of the thesis

With the background given, the aim of this thesis is to understand the local structure and dynamics of the MOF called CTH-17, using Raman spectroscopy and INS. More specifically the thesis seeks to give answers to the following questions:

i Do measurements of vibrational spectra with temperature variation show any changes that can be assigned to structure changes related to the gate opening effect observed in ref. [9]?

ii Do the vibrational modes correlate with the structural properties determined by SCXRD, and the rotational dynamics of the phenyl rings as determined by QENS?

iii What is the temperature threshold for the possible onset of the rotation of the phenyl rings in the CPB linker?

To have a similar material to compare with, another MOF that has previously been synthesized by Lars Öhrström, but not yet published, made of the same linker but with Lanthanum exchanged for Cerium, has also been analysed. This comparison can be expected to give information about how the type of rare-earth ion affects structure and vibrational dynamics of the novel type of MOF material.

1.3 Outline of the thesis

The thesis will begin with an introduction to MOFs (Chapter 2), with a specific focus on the key questions as addressed. This will be followed by a description of the experimental techniques used (Chapter 3), and experimental setups (Chapter 4). The results are presented in Chapter 5, and the conclusions in Chapter 6.

2

Metal Organic Frameworks

2.1 General structure and functional properties

MOFs are often described as porous crystals constructed of a network of metal ions linked with organic molecules. This is of often the case, but MOFs do not need to be crystalline, or even porous. The defining characteristics of MOFs is that they are solids constructed by a network with metal ions or metal clusters acting as nodes, connected with organic ligands [10]. The ligands can have varying size and complexity. They are often made up of complex structures of phenyl rings, with two sites or more (ditopic or polytopic), terminated with carboxylates or imidazolates making them negatively charged. The negative charges are compensated by the positively charged metal ion parts in the framework. With the freedom to choose and combine different metal-ions or organic ligands, a vast variety of different MOFs can be constructed with varying size, shape, pore-size and topology. An example of an extensively studied and cited MOF material is MOF-5 (also called IRMOF-1), discovered by Omar Yaghi, made of 1,4-benzodicarboxylate (terephthalic acid) organic linkers, and Zn_4O metal nodes [11]. It is named after the series of similarly structured MOFs with different lengths of the organic linker molecules giving them different pore sizes. MOF-5 was one of the first MOF candidates studied to be used for hydrogen storage, but is now also being studied to be used for catalysis, and sensing technologies [12] [13]. Another example is the zeolite imidazolate frameworks (ZIFs) series of MOFs. They are a collective of MOFs, where the organic linker have a imidazole group. ZIF-8 is frequently cited, made up of tetrahedral units with Zn ions connected with 2-dimethylimidazole linkers. They are currently studied for usage in CO_2 separation and adsorption [14]. Figure 2.1 illustrates the crystal structure of MOF-5 and ZIF-8 respectively.

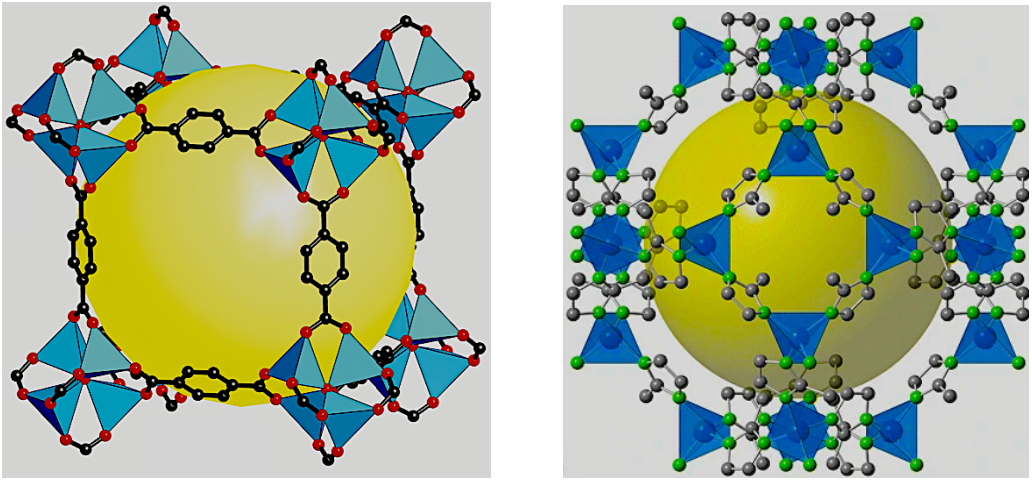

(a) MOF-5 **(b)** ZIF-8

Figure 2.1: Illustrations of the crystal structures of MOF-5 (a), and ZIF-8 (b). In both (a) and (b) the blue tetrahedrons have Zn in the center and represents the coordination of Zn to the linkers, the yellow spheres represents the pore volumes. In (a) the red and black dots are O and C-atoms, figure (a) is reproduced with permission from ref. [15], Copyright (2007) American Chemical Society. In (b) the green and black dots are N and C-atoms, figure (b) is reproduced with permission from ref. [16], Copyright (2016) Springer-Verlag Berlin Heidelberg.

The theoretical building blocks of MOFs are typically not what is directly added to the pot when making them, but they are theoretically built up by what is called secondary building units (SBUs) [17]. The organic SBU is simply the organic linker that binds to the metal SBU. The organic SBU (the linker) is often the deciding unit for the topology of the MOF. For MOF-5 and ZIF-8 the metal SBUs are the Zn^{2+}ions, acting as nodes, seen as blue tetrahedrons in Figure 2.1. Both of them have simple organic linkers with only one phenyl ring in the terephthalic acid, and one imidazole ring in the imidozolate as seen in Figure 2.1. The linker in CTH-17 consisting of CPB is more complex whith six phenyl rings, each connecting to two La(III) metal SBU acting as nodes. These parts are highlighted in Figure 2.2.

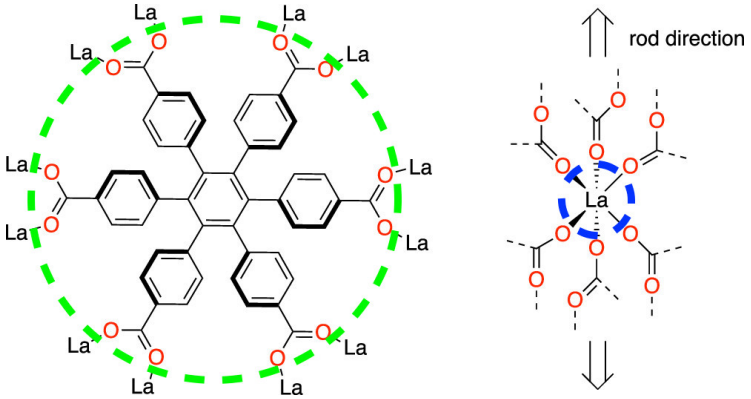

Figure 2.2: Figure 1.1 with highlighted areas of the SBUs in CTH-17. The green dotted area is the organic SBU, the blue dotted area is the metal SBU.

2.2 Synthesis routes towards MOFs

A common method of synthesis for MOFs is solvothermal synthesis, which is also the method used in this study. The reaction takes place in a closed vessel that can afford high pressure, which enables temperatures above the boiling points for the reactants and solvents. This in turn leads to higher solubility of the added components, and facilitate the desired reactions [10]. Typically the reagents are mixed together with a so called modulator, and a solvent such as dimethylformamide (DMF). The modulator is often a short ligand such as acetic acid, that competes with the linker molecules to bind to the metals. This can be used to control the reaction rate of the MOFs, which is a way of controlling the crystal sizes. A known problem when using DMF is that it can get hydrolyzed and break down into formic acid and methylamide. Formic acid has a OH group that can de-protonate and bind to charged metal ions, as in this case La^{3+} or Ce^{3+}. Those can bind to three formic acids and form Lanthanum Formate and Cerium Formate, which is not wanted in the synthesis of La_2(CPB) and Ce_2(CPB). Another important thing to mention regarding DMF is that it can get incorporated into the structure of the MOF and get stuck in the pores. Figure 2.3 shows how DMF is stuck in the pores of CTH-17. A simple way of removing DMF from the MOF is to simply heat it to temperatures that breaks the bonds of the oxygen in DMF that is coordinated to the metal ions in the MOF, but below temperatures that breaks down the MOF crystal structure. Once the solvent is removed from the pores (in our case the DMF), the MOF is said to be "Activated".

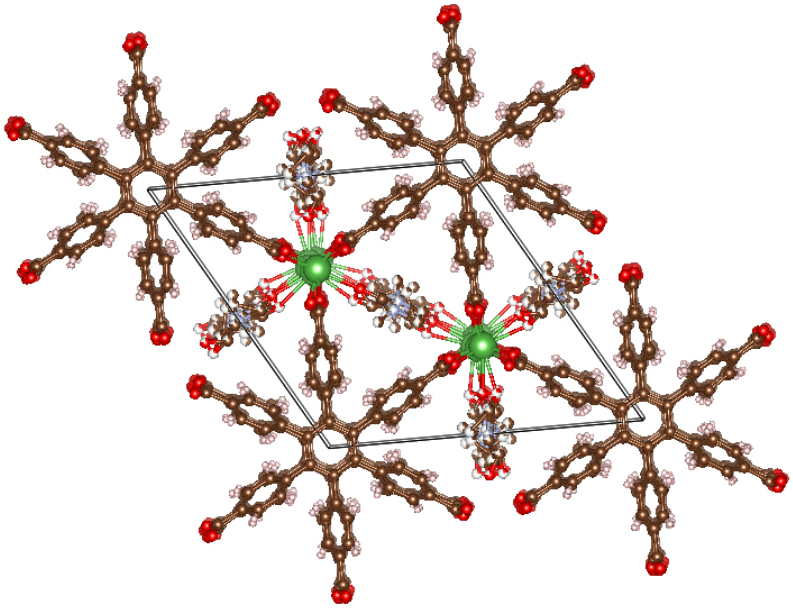

(a) La_2(CPB) (CTH-17) with DMF in the pores (Unactivated).

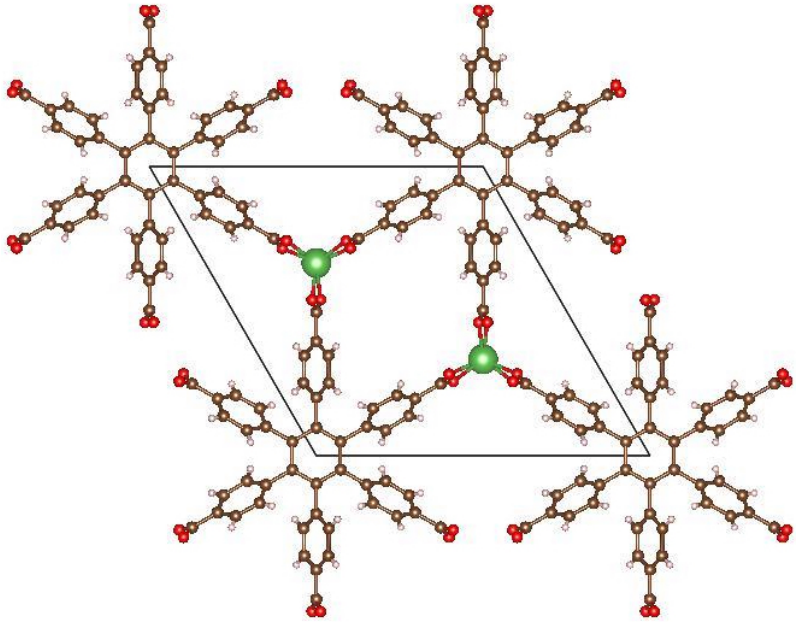

(b) Activated La_2(CPB) (CTH-17).

Figure 2.3: Two structures of CTH-17, (a) with DMF in the pores, and (b) without DMF in the pores. Brown, white, read and green dots are carbon, hydrogen, oxygen and lanthanum atoms. The light blue dots are nitrogen atoms in the DMF. The figures were generated with public CIF data accessed on Cambridge Crystallographic Data Centre (CCDC) website [18], using VESTA software [19].

2.3 Flexible MOFs

Some MOFs are only stable when a guest molecule is incorporated into the structure, others are stable both with and without guest molecules, and some are flexible. These are referred to as the first, second, and third generation of MOFs, illustrated in Figure 2.4. Flexible MOFs, or ”soft” MOFs, describe MOFs that are able to change their own framework in response to external stimulus such as guest molecules, heat, light or pressure. The pores of these MOFs can mechanically open up in response and change the entire molecular structure, increase the total surface area of the MOF, and give rise to new properties such as to selectively encapsulate certain particles. Understanding of this phenomena is ongoing research, but so far researchers have observed structurally different ways on how it occurs, and been able to categorize some flexibilities. In Figure 2.5, four of the most accepted definitions of MOF flexibility is presented. The most noticed MOF flexibility with plenty of related publications is the breathing effect. This was first observed in 2004 by the group of S. Kitagawa and G. Ferey [20]. This occurs due to what is known as foldable network topology, a topology where the metal SBUs act as nodes that the attached linkers move freely around, and ”folds” the structure [17].

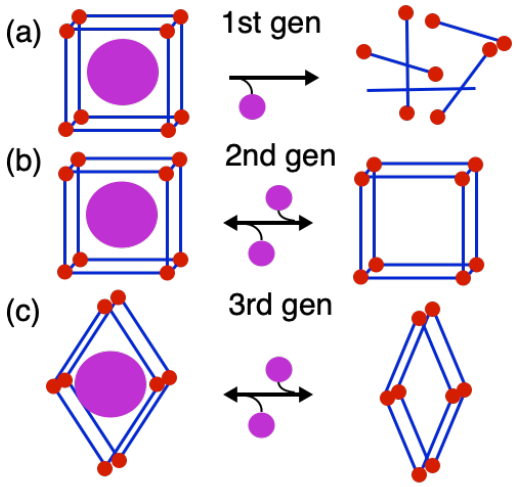

Figure 2.4: (a) Schematic visualization of framework collapse when the guest molecule in purple leaves, known as the first generation compound; (b) Schematic visualization of the more stable framwork that does not collapse when guest molecule enters or leaves, known as the second generation compound; (c) Schematic visualization of a flexible framework, known as the third generation compound. The figure is adapted from ref. [21].

Another common type of flexibility is the swelling effect, where a gradual enlargement of the unit cell takes place, typically because of interactions with guest molecules. The unit cell becomes bigger with no bond breakage, and enables molecules to enter or leave easier [7]. Subnetwork displacement can happen when two or more networks are weakly bonded by van der Wahls interaction and can relocate and shift in relation to each other. This includes stacked 2D networks, interpenetrated 3D networks and interdigitated 2D networks [22]. Linker rotation flexibility is when the spatial alignment of the linker is rotated [8]. However, it is not always as simple as that. In a crowded atomic-scale environment there are multiple forces acting on each molecular part, making a dynamically complex environment. The linker rotation in the material in this study, La_2CPB, seems to make the structure stretch along the rod direction, or only be possible if the structure is stretched out as mentioned in chapter 1.1. A combination of the mentioned flexibilities must therefore not be ruled out.

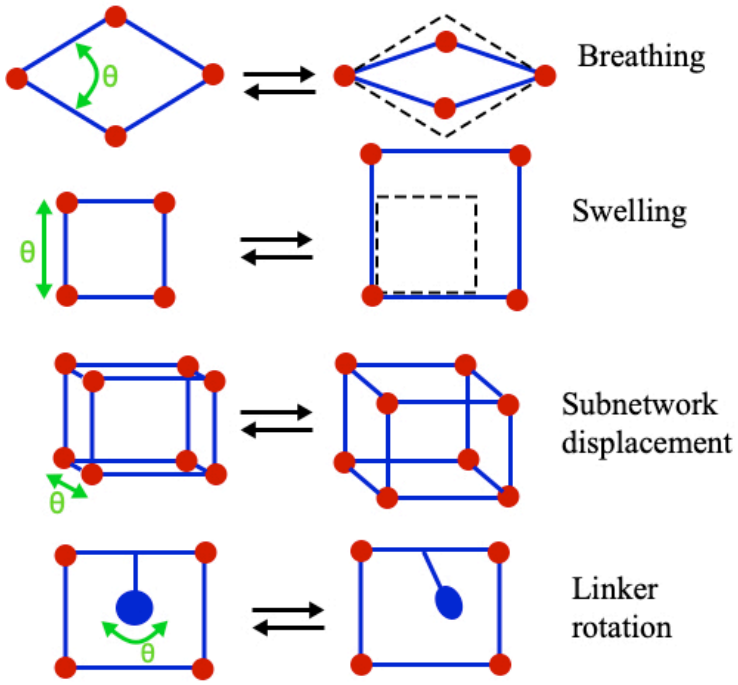

Figure 2.5: Illustrations of breathing, swelling, subnetwork displacement, and linker rotation flexibility. The figure is adapted from ref. [23].

2.4 CTH-17 and Ce_2CPB

CTH-17 consists of La(III) metal SBUs and the hexagonal shaped linker 1,2,3,4,5,6-hexakis(4- carboxyphenyl)benzene (CPB), La_2(CPB). Ce_2(CPB) has La(III) exchanged for Ce(III). CTH-17 reacts to temperature increase or to increase in gas pressures by changing the structure. Figure 2.6, shows the structure at 90 K when viewed along the rod direction, measured with SCXRD. Each phenyl ring in the linker has the same chirality, meaning that they are slightly twisted in the same direction forming a propeller like structure, indicated with the yellow arrow in the figure. When the temperature is increased to some threshold value between room temperature and 500 K, the angle of the twisting changes, and the rings become more "upwards standing" in the rod direction (the direction of the z-axis in Figure 2.6). For the rings to be able to twist, more space is needed since there is repulsion between the electron clouds of the rings and the surrounding atoms. This results in stretching of the structure along the rod direction, which generates bigger pores and more space inside the structure [9].

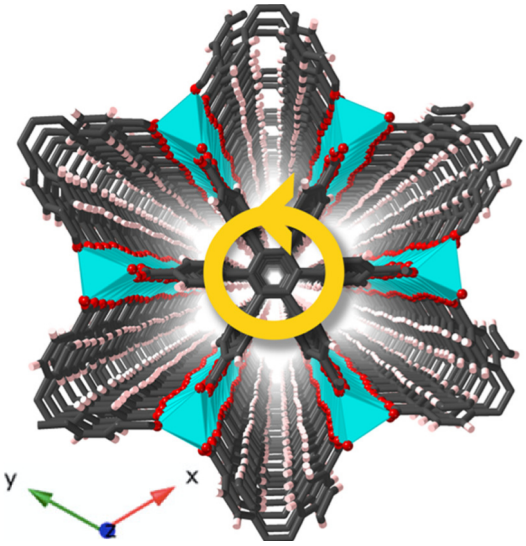

Figure 2.6: CTH-17 viewed in the stacking direction, with the CPB linker in the middle. The yellow arrow indicates the direction of the propeller like structure of the angled phenyl rings. The black colored structure represents carbon atoms in the CPB linker. The red dots connecting the trigonal blue parts are the oxygen atoms connecting to La atoms. White/pink dots are hydrogen atoms. The image is reproduced with permission from ref. [9], Copyright (2022) American Chemical Society.

Figure 2.7 shows images of the phenyl ring connected to the metal, generated with DFT calculations. The left image is for space group $P622$ present at room temperature, and the right image is for space group $P6/mmm$ present at temperatures around 500 K. When the sample changes from space group $P622$ to $P6/mmm$, the phenyl rings rotate by 15°, the two La-O bindings per phenyl ring becomes further apart and rotate 10°, and the La to La atomical distances increase. Figure 2.8 shows the void space between two La atoms (one of the voids between the six linkers seen in Figure 2.6). The void is clearly bigger for the structure with space group $P6/mmm$.

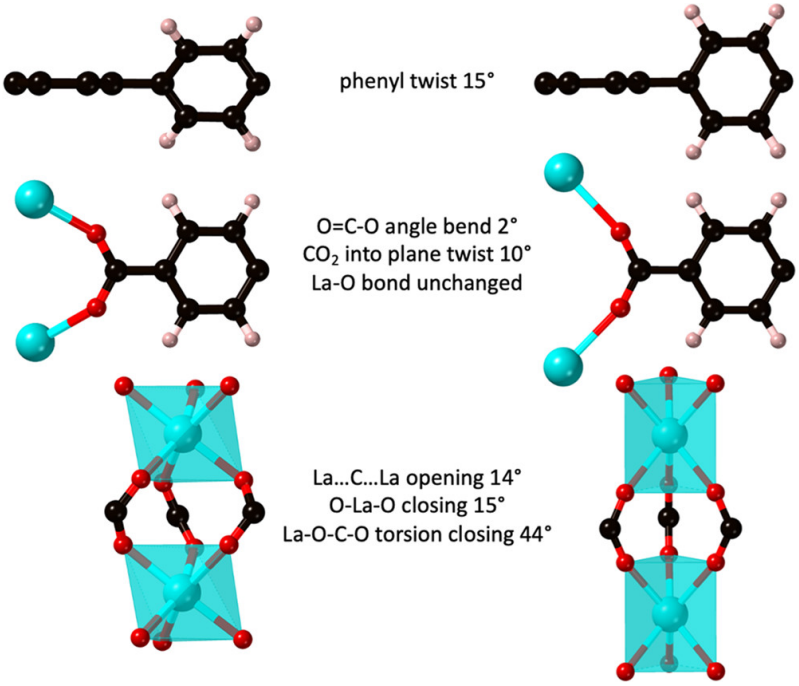

Figure 2.7: Generated figures of a phenyl ring from DFT calculations showing angular changes of the bondings. Left images are from an assigned structure with space group $P622$, and right images with space group $P6/mmm$. The black colored structure represents carbon atoms in the CPB linker. The red dots connecting the trigonal blue parts are the oxygen atoms connecting to La atoms. White/pink dots are hydrogen atoms. The image is reproduced with permission from ref. [9], Copyright (2022) American Chemical Society.

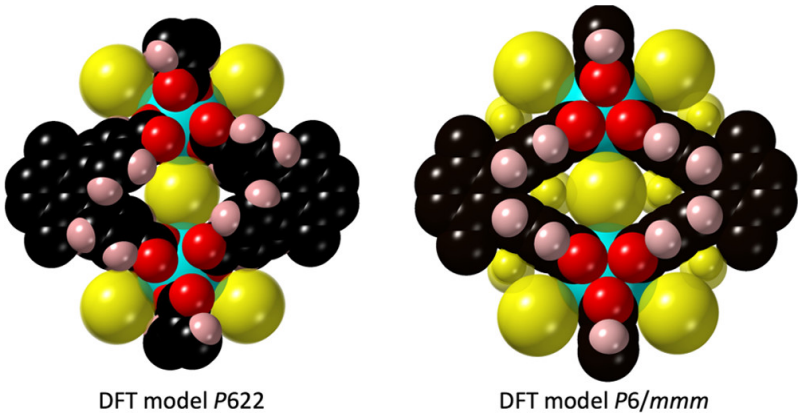

Figure 2.8: A visual representation of the increased void space when comparing the two structures with space group $P622$ and $P6/mmm$. The black colored structure represents carbon atoms in the CPB linker. The red dots connecting the trigonal blue parts are the oxygen atoms connecting to La atoms. White/pink dots are hydrogen atoms, and the yellow spheres represents the void space. The image is reproduced with permission from ref. [9], Copyright (2022) American Chemical Society.

3
Methods

In this thesis the overriding goal has been to detect and analyse local atomic vibrations in CTH-17 when the structure undergoes the changes seen in Figure 2.7 and 2.8, using Raman spectroscopy and INS. In the following of this chapter the basic theory of these methods will be briefly introduced. Some expected results of Raman and INS spectra will be explained based on the introduced theory. Particularly expected changes of Raman and INS spectra when the crystal structure of CTH-17 changes from space group $P622$ to $P6/mmm$ as described in the previous section.

3.1 Raman spectroscopy

In 1928 Chandrasekhara Venkata Raman together with Kariamanikkam Srinivasa Krishnan discovered inelastic scattering of light from organic liquids [24], the first observation of a phenomenon that today is extensively used by chemists and physicists all over the world. This scattering can give a fingerprint of the material being observed, and also information about the vibrational dynamics in the material. Figure 3.1 is a Jablonski diagram showing what happens with the energy from an incoming photon if/when a certain vibrational modes gets excited. The energy refers to the potential energy of an electron in an orbital, the energy amount corresponds to the amount of energy it would take to completely remove the electron from the orbital. If a vibration between one or more atoms in the material gets hit by the photon, the vibrating atoms get excited and "stores" the energy for a very short time, decided by the uncertainty principle, called a virtual state. The virtual state quickly undergoes deexcitation and releases the energy in form of a new photon, back to its original electronic state. The process is called Rayleigh scattering if it deecxites back to the original vibrational state as well, but if it deexcites to a higher vibrational state it is called Stokes Raman scattering, and anti Stokes Raman scattering if it deexcites to a lower vibrational state [25]. By detecting Stokes or anti Stokes scattering a spectrum that shows the various types of vibrational frequencies in a material can be obtained.

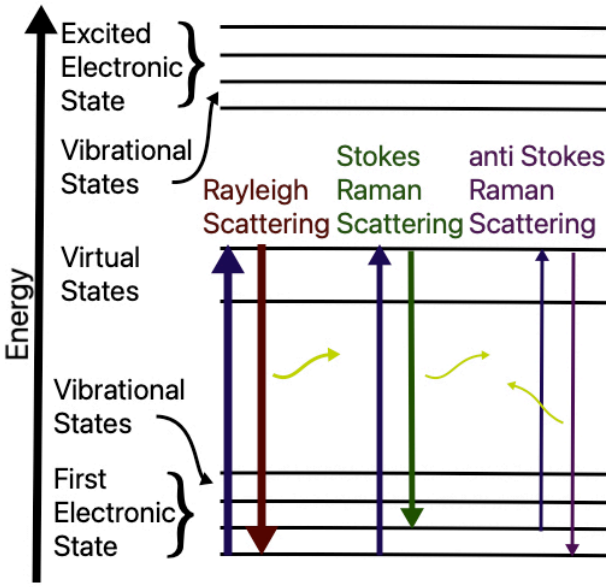

Figure 3.1: A Jablonski diagram explaining the Raman scattering effect.

3.1.1 Energy levels from oscillatory motions

Oscillatory motions of atoms, or vibrations in a material is a dynamic state formed by a complex interplay of attractive and repelling forces between atoms, held together by chemical bonds. A simplified way of describing oscillatory motion between two atoms bound to each other is to compare it with a spring. An oscillating spring repeatedly exchange potential energy to kinetic energy, just like two vibrating atoms. Vibrating atoms are acting in such small dimensions that quantum mechanical effects obey, and the vibrational states have discrete quantified levels, as in Figure 3.1. By using Hooke's law and the Schrödinger equation, the total energy of the system (potential energy plus kinetic energy) for a certain vibrational energy state can be obtained with the following solution:

$$E = h\nu\left(n + \frac{1}{2}\right) = h\left(n + \frac{1}{2}\right)\frac{1}{2\pi}\sqrt{\frac{k}{m}}. \tag{3.1}$$

Here ν is the classical vibration frequency, k is the spring constant reflecting the bond strength between the atoms, h is the planck constant, m is the reduced mass of the system, and $v \in 0, 1, 2...\infty$ is the vibrational quantum number. In reality though, a better approximation of the potential energy between two atoms separated with a distance r is the empirically-derived Morse potential:

$$U = D_e(1 - e^{-\beta r}). \tag{3.2}$$

Here D_e is the dissociation energy and β is an empirically measured constant. With this taken into account the vibrational energy states in Figure 3.1, can be visualized in relation to the distance r between the atoms, see Figure 3.2. Once Stokes or anti Stokes Raman scattering occur due to some transition between the vibrational states as earlier described, a peak occurs at the wavelength for the respective energy state transition in the Raman spectrum.

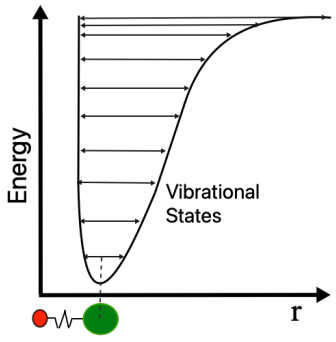

Figure 3.2: A visual representation of energy states with a Morse potential for a diatomic system.

3.1.2 Molecular vibrations and Selection rules

Vibrations between two bonded atoms is just one out of many more possible diatomic or multiatomic vibrations in the structures. In a triatomic molecule such as a methylene group (CH_2), vibrations such as streching, scissoring, rocking, wagging and twisting are possible, and for stretching it can be both symmetric and anti symmetric, see Figure 3.3. Vibrations for molecules with more than three atoms are even more complex to describe. In 3D space the total number of vibrations for a solid compound with N atoms is 3N-3, these are called optical modes or optical phonons. The 3 subtracted vibrations are from uniform translational motions of the entire solid, these are called acoustic phonons (at the Γ-point in the Brillouin zone of a unit cell, the frequency of the acoustic phonons are 0, which equals uniform translational motions of the entire unit cell. These modes are not detectable with Raman or IR spectroscopy) [25]. In one unit cell of CTH-17 there are 86 atoms. That means that there are $3 \cdot 86 - 3 = 255$ vibrational modes in only one unit cell. However, not all of the vibrations are "Raman active", because certain selection rules apply. These rules will be explained in the next section.

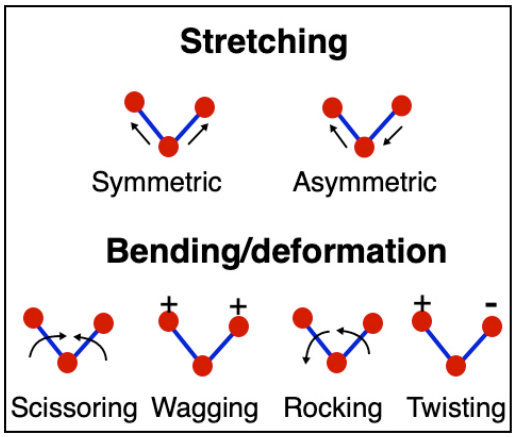

Figure 3.3: Normal modes of vibrations in a triatomic molecule.

3.1.2.1 Selection rule theory

Raman scattering occurs due to interaction of light with the electron clouds, and not with the atomic nuclei as in the case of neutron scattering that will later be explained in Section 3.2. An excitation of a vibrational state is an excitation of the electrons in the electron cloud of the associated vibration. The cloud becomes an induced electric dipole, which in turn causes a polarization current, which leads to scattering. A detailed mathematical derivation of the dipole moment induced by an incoming photon (electromagnetic wave) is beyond what is necessary for this study. In short the induced electric dipole moment p is dependent on the incoming electromagnetic field E and the polarizability α of the molecular vibration, and they are related according to the following expression:

$$p = \alpha E. \tag{3.3}$$

The polarizability is a measure of the tendency of a molecule (or in our case a vibrational mode of a molecule) to generate an induced electric dipole moment when subjected to an electric field. When there is a change of vibrational states, the polarizability must also change. That means that no symmetrical vibrations where the polarizability change is equal to zero with respect to its equilibrium internuclear separation will give any Stokes or anti Stokes scattering [25]. Since there is a lot of symmetry in the structure of CTH-17, there will not be 255 bands in the Raman spectrum. Figure 2.1 in Section 2.2 shows the complexity of atoms in the CTH-17 structure, and also symmetry that occurs. However it is very difficult to point out which type of vibration will be symmetrical or not in such a complex structure (Ce_2CPB is practically identical to CTH-17, with La exchanged for Ce-atoms). Notice for instance that La is bound to 6 oxygen atoms, meaning that it is not as simple as to expect polarizability changes between only these two atoms and calculate the wavelength of scattering from a single La-O vibration. In an atomically crowded space, vibrations gets affected by attractive forces from surrounding atoms as well.

3.1.3 Expected bands

By looking at studies of similar materials some vibrations are expected to be found in CTH-17 and Ce_2(CPB), for instance the vibration between the metal-ion (La or Ce) and oxygen [26]. La and Ce have different masses and different structure charges when ionically bonded in the MOF (La with 57 protons weigh 138.90547 u, and Ce with 58 protons weigh 140.116 u) which changes the frequency of the vibration.

A lot of scattering will come from different combinations of C−C and C−H vibrations in the aromatic rings, since they are the most frequently occurring bonds in the structure. There are 30 fundamental vibrations only from the benzene rings, the frequencies for all these vibrations can be calculated with DFT calculations, and simulated Raman spectra can be obtained [27][28]. It is difficult to visually show vibrational motions in complex multi-atomic moleculus such as benzene rings, but there is a website showing all 30 vibrational motions of a benzene ring in free space, made by John J. Nash [29]. These frequencies can be used as a reference to compare with Raman spectra from the structure in Figure 2.3. However, they will be different from the bands in the Raman spectrum since the vibrations are, as mentioned, in an atomically crowded environment which will shift the frequencies and may alter the shape of the bands. Additionally to the internal vibrations between atoms in the phenyl rings, the whole 2D-molecules themselves will also vibrate. They will either do full rotations, or they will do a torsional waggling motion back and forth, called libration, see Figure 3.4.

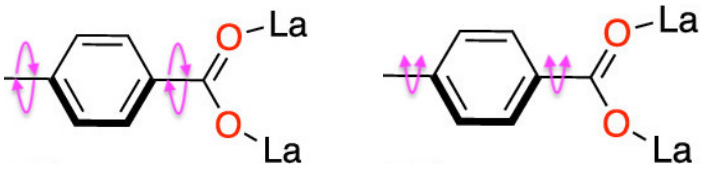

(a) Rotation. **(b)** Libration.

Figure 3.4: Motion illustrations of phenyl ring rotation (a) and phenyl ring libration (b). The motions are indicated with the pink arrows. The phenyl ring is one of the phenyl rings in the CTH-17 structure in Figure 1.1.

Vibrations of the phenyl rings are interesting to follow during temperature variation, since the crystal structure of CTH-17 is supposed to have the phenyl rings rotated 15° in the structure belonging to space group $P6/mmm$ found at 500 K, compared to the structure consistently found in 300 K belonging to the chiral space group $P622$, as mentioned in section 1.1. Alexander E. J. Hoffman et al., made DFT calculations and Raman spectroscopy measurements on a MOF called DUT-8 with four different metal nodes, Ni, Cu, Zn and Co [30]. The molecular structure is different from CTH-17, it is cubic and have 2,6-naphthalen dicarboxylic (2,6-ndc) linkers with two benzene rings, see the illustration of DUT-8 in Figure 3.5. The structure has two modes, "open" and "closed", where the linker has rotated in the latter mode. They calculated and spectroscopically showed that active linker rotation frequency would be at 21 cm^{-1} in the closed mode, and at 60 cm^{-1} in the open mode. Considering the double benzene rings in the linker making them heavier than the phenyl rings in CTH-17, the energy of an eventual CTH-17 linker rotation should be lower and therefore have higher frequency. However, this motion would not be much different from a potential rotation or libration of the phenyl rings in CTH-17, and a band with a frequency in the vicinity of 21-60 cm^{-1} is expected. It is difficult to conclude with SCXRD measurements if (in this case) phenyl rings are fully rotating or librating, since this instrument generates a calculated average position of the atoms, and therefore an average static crystal structure. The same goes for DFT calculations when calculating an average static crystal structure. This was how the crystal structures of CTH-17 were assigned and calculated in the study in ref. [9]. The phenyl rings could for instance librate in lower temperatures, and start fully rotate in higher temperatures. Or perhaps be rotating for all temperatures, but change in frequency depending on the temperature.

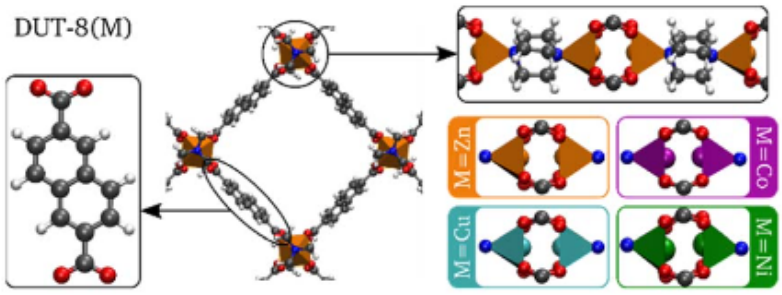

Figure 3.5: DUT-8 with a zoomed in image of the 2,6-ndc linker, and a zoomed in image of the metal SBUs and how they are connected with 1,4-diazabicyclo[2.2.2]octane (Dabco) in the stacking direction. The figure is reproduced with permission from ref. [30], Copyright (2023) The Royal Society of Chemistry.

The bands in the Raman spectra will be carefully analyzed, particularly the ones that are related to phenyl ring rotations or librations, and the stretching of CTH-17 in the rod direction. They will also be analyzed by comparing them for CTH-17 and Ce_2(CPB). When the temperature is varied during measurements the bands can shift in frequency, become wider, increase in intensity, and new bands can show up when structural changes occur. A shift in frequency could be because of changes in the environment around the vibration affecting the frequency, as mentioned earlier. Bandwidth changes can also occur during structural changes, uniformity of bond lengths gives narrow bands which for instance can indicate high crystallinity. New bands is expected to show up when temperature is varied and excitations of new vibrations becomes possible due to the thermal energy input. An example of temperature variational Raman spectroscopy analysis can be found in ref. [31]. In this papar a temperature sweep between 133 and 533 K was made on a triple layer of WSe_2 and a sequence of 11 Raman spectra were measured. Figure 3.6 shows a chosen region of a band of symmetry E^1_{2g}. Notice how the band gets wider with higher temperature, and a new band appears. Additionally the right image clearly shows a frequency shift of the band.

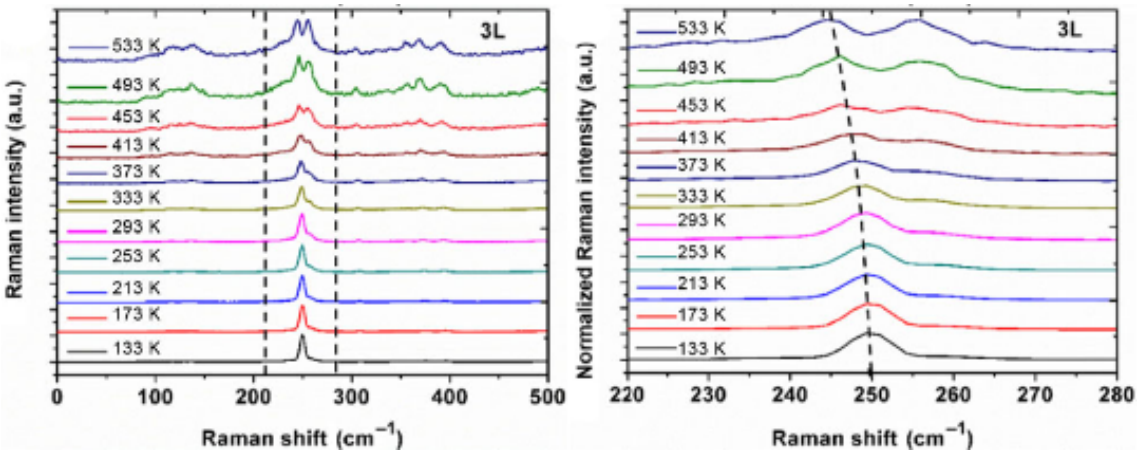

Figure 3.6: The left image shows variable temperature Raman spectra, and the frequency range with the band from E2g vibrations is indicated with two vertical dashed lines. The right image shows the spectra zoomed in on the frequency range, with a dashed line following the frequency shift of E2g vibrations. The figure is reproduced with permission from ref. [31], Copyright (2020) Tsinghua University Press and Springer-Verlag GmbH Germany, part of Springer Nature.

3.2 Inelastic neutron scattering

In neutron scattering spectroscopy, a beam of neutrons is shot on the sample. This may be compared to Raman spectroscopy, where photons are shot on the sample and interact with the electron clouds, and changes of the electron cloud polarizability is needed for a scattering event to occur. Neutrons interacting with the nucleus have no such restrictions for scattering to occur, meaning that there are no selection rules. INS arises when neutrons hit the nuclei of the sample, and energy (E_t cm^{-1}) and momentum ($\boldsymbol{Q}$,$|\boldsymbol{Q}|$=Q Å^{-1}) are transferred to the material. E_t and $\boldsymbol{Q}$ are measured by simply comparing the initial, i, energy and momentum of the neutrons with the collected final, f, neutrons.

$$E_t = E_i - E_f, \qquad \boldsymbol{Q} = k_i - k_f. \tag{3.4}$$

Here $k = 2\pi/\lambda$, where λ is the wavelength of the neutron. Figure 3.7 shows a simplistic illustration of what is being measured, the observables. The figure only illustrates neutrons that actually interact with the sample and lose energy. In reality most of the neutrons are not scattered by the sample.

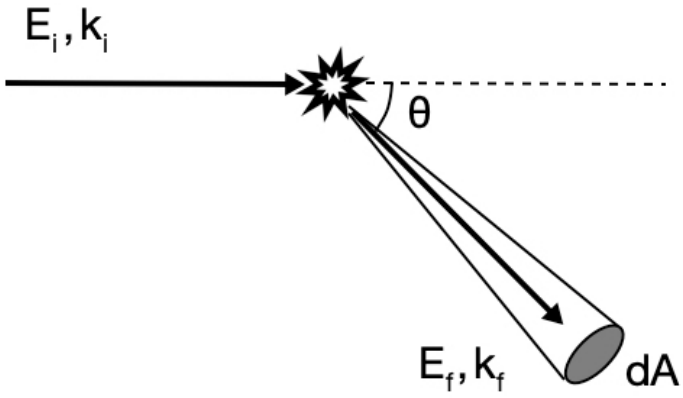

Figure 3.7: An illustration of incoming neutrons of initial energy and momentum E_i, k_i, striking a sample, scatter with an angle θ, and hitting a detector with an area dA at distance d from the sample.

To theoretically describe how the exchange in energy is related to vibrations in the measured material it is necessary to use quantum mechanical expressions. However that kind of thorough descriptions of the physics behind it is more than what is necessary for this study. The book "Vibrational Spectroscopy with Neutrons" by Philip C H Mitchell et al., gives detailed theoretical explanations [32]. For this study a simplified form of the equation called The Scattering Law, that describes what factors determines the intensity of the measured signal is presented. It is enough to explain why some vibrations give stronger signals than others,

$$I_i \propto Q^2 U_i^2 e^{(-Q^2 U_{total}^2)} \cdot \sigma. \tag{3.5}$$

Here i denotes the ith molecular vibration transition, U_i is the amplitude of vibration, and U_{total} is the total mean square displacement of the molecule, σ is the inelastic neutron scattering cross-section for all the atoms involved in the vibration. The exponential term is called the Debye Waller factor, and it can make the signals become very weak if it is too high. Therefore U_{total} needs to be low, which can be done by reducing the temperature of the sample. That is why the samples have to be held at very low temperatures during the measurements, which limits the possibilities to make temperature variational INS measurements, as with the Raman spectroscopy. Another important thing to mention regarding the cross-section value σ for certain vibrational modes is that hydrogen atoms alone have a very large cross-section value compared to all other atoms. This means that typically, all vibrations with hydrogen atoms involved will give the strongest signal [33].

4

Experimental

4.1 Synthesis of La_2(CPB) and Ce_2(CPB)

The synthesis of La(III) 1,2,3,4,5,6-hexakis(4- carboxyphenyl)benzene (La_2(CPB) or CTH-17), and Ce(III) 1,2,3,4,5,6-hexakis(4- carboxyphenyl)benzene (Ce_2(CPB)) involved heating and stirring of the reagents for approximately 20 to 30 minutes in 120 °, together with acetic acid acting as a modulator of the reaction, and DMF as solvent. The liquid was then transferred to a Teflon-lined, stainless-steel autoclave, and kept in an oven for 8 days in 150 °C. A white powder could then be filtrated out of the liquid, and washed with DMF. Figure 4.1 shows images of the autoclave, the Teflon container and an example of the white powder product. The followed steps and the amounts of reagent, modulator and solvent was the same as described in Francoise M. Amombo Noa et al. (Found in Supporting Information, the second route described) [9]. Here is a description of the followed steps:

Measured 0.1 g (0.125 mmol) of H_6cpb was dissolved in 40 ml of DMF under stirring at 120řC in a glass beaker. Once heated, 0.2165 g (0.5 mmol) of lanthanum/cerium nitrate hexahydrate ($La(NO_3)_3$/$Ce(NO_3)_3$), and 10 ml of glacial acetic acid was added, and the mixture was left to stir. The solution was then transferred to a Teflon-lined, stainless-steel autoclave, and then transferred to a preheated Memmert UN75plus oven at 150 °C. The sample/samples stayed in the oven for 8 days. A white participate was formed, containeing the MOF. It was filtered and washed three times with 10 ml of DMF each time, and left to dry. A white powder with small white crystals appeared.

For synthesis of Ce_2(CPB) the same procedures was made, but with different calculated masses of added Ce-salt crystals to get the same molar mass ratios. However since the molar mass difference between La and Ce is only 1.21053 u and the wanted molar ratios was 0.5 mmol, the difference in grams were in the 10^{-3} g ratio which is undetectable for the used weighing scale. In the first synthesis, three batches of Ce_2(CPB) were made and two batches of La_2(CPB). In the second synthesis, two batches of Ce_2(CPB) were made and three batches of La_2(CPB). In the third synthesis one batch of each was made with doubled amounts of everything.

(a) Autoclave plus Teflon container.

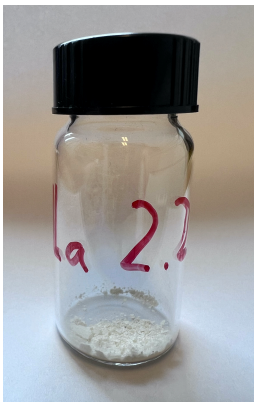

(b) Powder product.

Figure 4.1: Image (a) shows the stainless steel autoclave and the Teflon container. The Teflon container with the liquid is put into the autoclave. Image (b) shows an example of a white powder product with La_2(CPB) crystals.

4.2 Powder X-ray Diffraction analysis

The crystal structure and phases formed in the synthesis product was determined by PXRD. A Bruker D8 Discover diffractometer operating with Cu Kalpha radiation was used [34]. The powders were placed on a Si crystal zero background sample holder and measured over the 2θ interval 0 to 45 degrees. The diffractograms were compared to calculated diffractograms made in VESTA software with CIF information of the La_2(CPB) crystal structure from the paper by F.M. Amombo, L. Öhrström et al., and handed over CIF information from professor Lars Öhrström of the Ce_2(CPB) crystal structure [19][9]. They were also compared to calculated diffractograms of La and Ce formate, a known impurity from earlier synthesis and SCXRD measurements by professor Lars Öhrström, also made in VESTA software with handed over CIF information from Lars Öhrström.

4.3 Scanning Electron Microscope imaging

SEM imaging was used to image one La_2(CPB) sample. The SEM instrument used was a LEO Ultra 55 [35]. To make the sample conductive it was sputtered with gold before it was put into the SEM.

4.4 Raman spectroscopy measurements

The Raman spectroscopy instrument used in this study was a Renishaw InVia confocal Raman microscope with a connected 785 nm laser [36]. During temperature variational measurements, a heating stage of the type Linkam THMS600 System was used [37]. For every measurement a small piece of the sample was placed on an aluminum cup holder under the microscope. Focal points for the 785 nm laser beam was chosen with the microscope by zooming in on an appropriate spot. The first measurements were carried out in room temperature for both unactivated and activated samples of La_2(CPB) and Ce_2(CPB) during one occasion. For the temperature variational measurements, a new sample was placed on the holder before every new measurement with a temperature sweep. This was to make sure that no irreversible changes in the material affected the measurement results. The temperature was sweept down to -100 °C, which was the lowest possible temperature, and then up to 400 °C. For every 50 °C, a Raman measurement was made. One sequence of measurements from -100 to 400 °C with 50 °C steps, took approximately 1 hour. The reason for stopping at temperature 400 °C was because the samples turned out to give a strong photoluminescence background, and started to saturate the photo-detector for higher temperatures. All measurements were controlled from a computer, including the temperature of the heating stage with a connected pump for liquid nitrogen supply. Cooling water was also connected to the Linkam stage at all times to avoid damage to surrounding instrument parts.

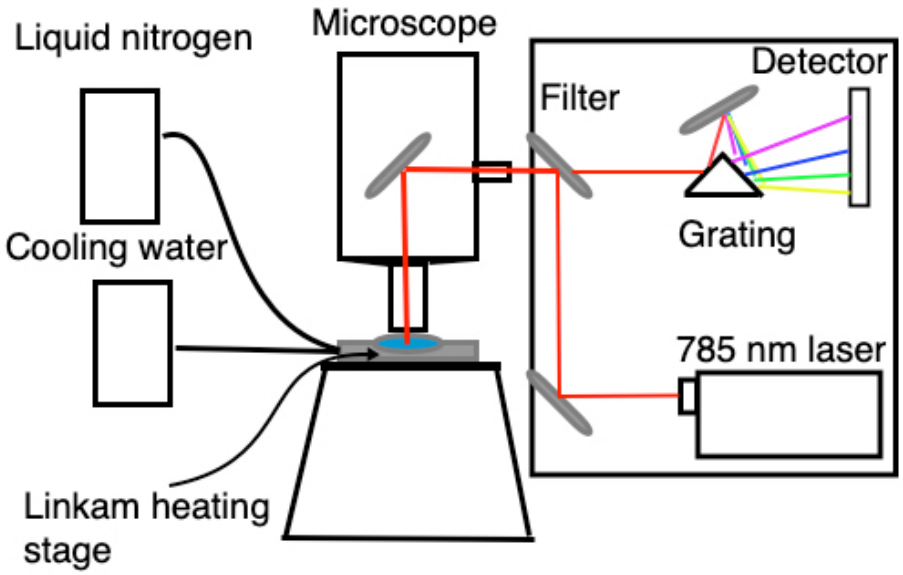

Figure 4.2: Schematic figure of the Raman spectrscopy setup with the sample placed inside the Linkam stage.

4.5 INS measurements with TOSCA

The INS measurements were performed on the instrument called TOSCA, at the ISIS Pulsed Neutron and Muon Source, in the U.K. The five batches of La_2(CPB) samples were mixed together, and the five batches of Ce_2(CPB) samples were mixed together, with masses of approximately 0.6 g for the La_2(CPB)-mix and 0.69 g for the Ce_2(CPB)-mix. Each mix was placed into a sample cell, and measured in standard atmosphere pressure (101,325 Pa) and air. The measurements were performed in 10 K which was maintained with a cryostat. Figure 4.3 shows cross-section images of the detector modules and the cryostat. Fired pulses of neutrons onto the sample cause them to forward scatter and back scatter. At angles of 45 ° and 135 ° from the incident neutron beam there are analysers equipped with graphite crystals that Bragg scatters neutrons with one specific wavelength, or mutliple of that wavelength, according to Braggs law. These neutrons are passed through a beryllium filter that filter out a range of wavelength multiples, and finally they are detected at a time T. The time T is also called time of flight, and it is related to the momentum and energy transfer between the neutron and the sample. Therefore a spectra can be obtained with the detected scattered neutrons (intensity) per energy transfer. Measurements were made over the energy transfer interval -20 to 8000 cm^{-1}. Data was analyzed in the range of 15 cm^{-1} to 4000 cm^{-1}.

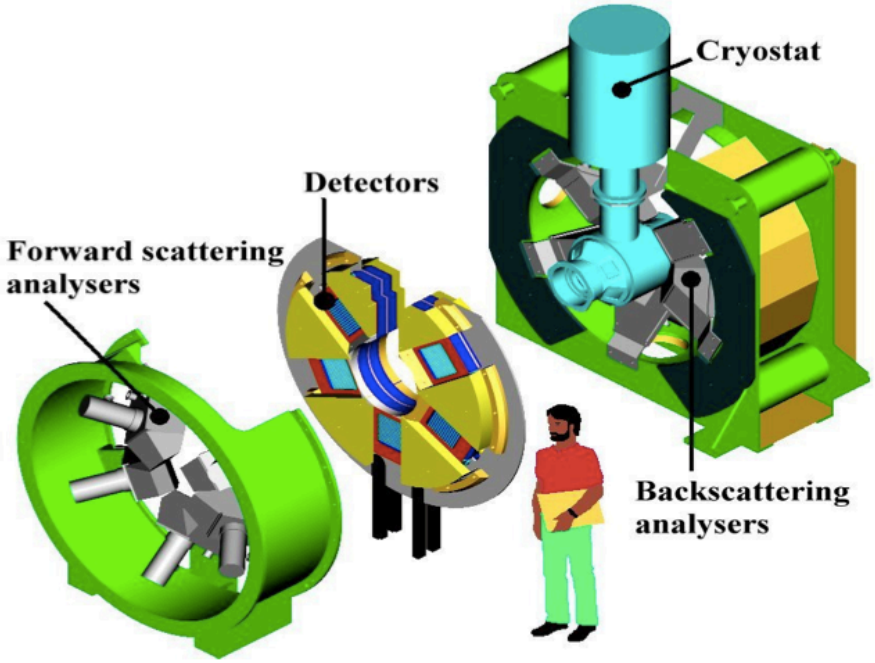

Figure 4.3: Schematic figure of TOSCA. Image is reproduced from ISIS Neutron and Muon source TOSCA user manual, see ref. [33].

5
Results

5.1 Synthesis and average structure determination

The peaks in the diffractogram in Figure 5.1 from the sample correspond well with the calculated diffractogram, and it is safe to say that the sample contains the desired La_2CPB crystals. The difference in intensity in some of the peaks could be because of variations in crystal size and orientation in the sample. However, their positions on the 2θ-axis (x-axis) are accurate, indicating a pure crystalline sample. The same diffractograms were made with samples from the other batches and compared with the calculated diffractograms, and the results varied. Undesired Lanthanum formate or Cerium formate was formed in most of the batches. To see to what extent it had been formed in every batch, diffractograms from the batches were compared with calculated diffractograms of Lanthan formate and Cerium formate. Figure 5.2 shows the comparison for a Lanthanum sample. The peaks at 16, 28, 34, and 42 degrees correspond well with each other indicating that the sample contains Lanthanum formate. All batches except the first one made contained La/Ce formate to some extent.

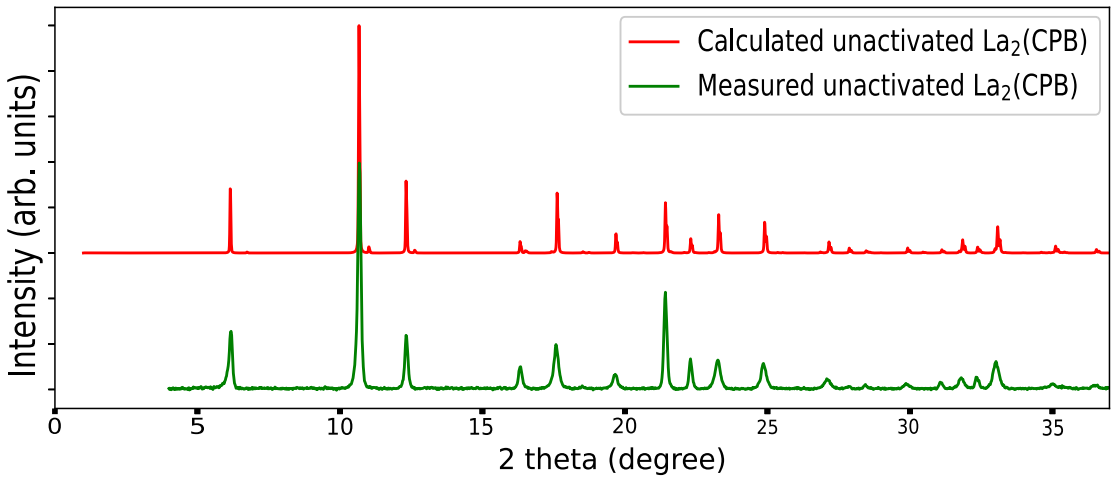

Figure 5.1: La_2(CPB) PXRD diffractogram in green, compared with calculated PXRD diffractogram in red. The background signal in the La_2(CPB) diffractogram was subtracted to make it flat.

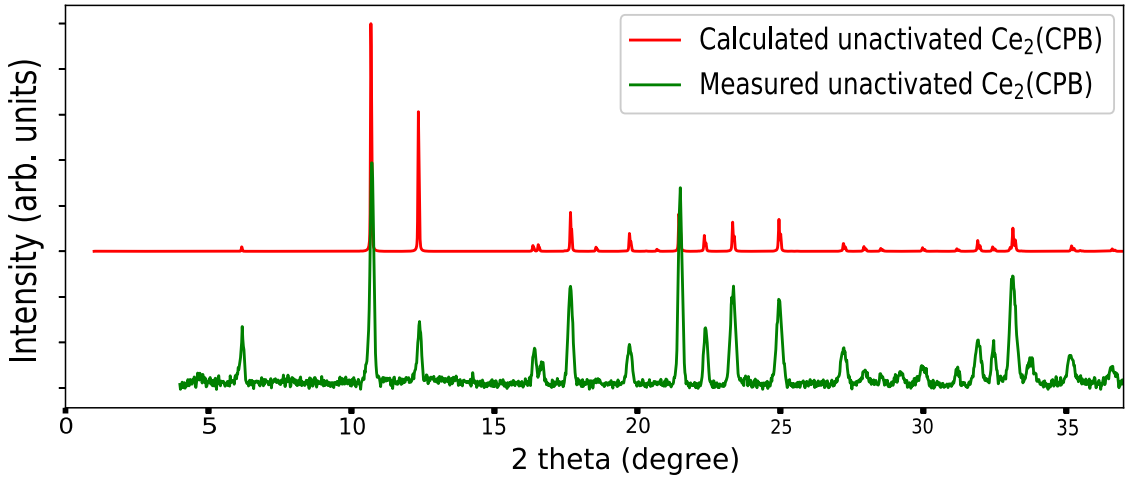

Figure 5.2: Ca_2(CPB) PXRD diffractogram in green, compared with calculated PXRD diffractogram in red. The background signal in the Ce_2(CPB) diffractogram was subtracted to make it flat.

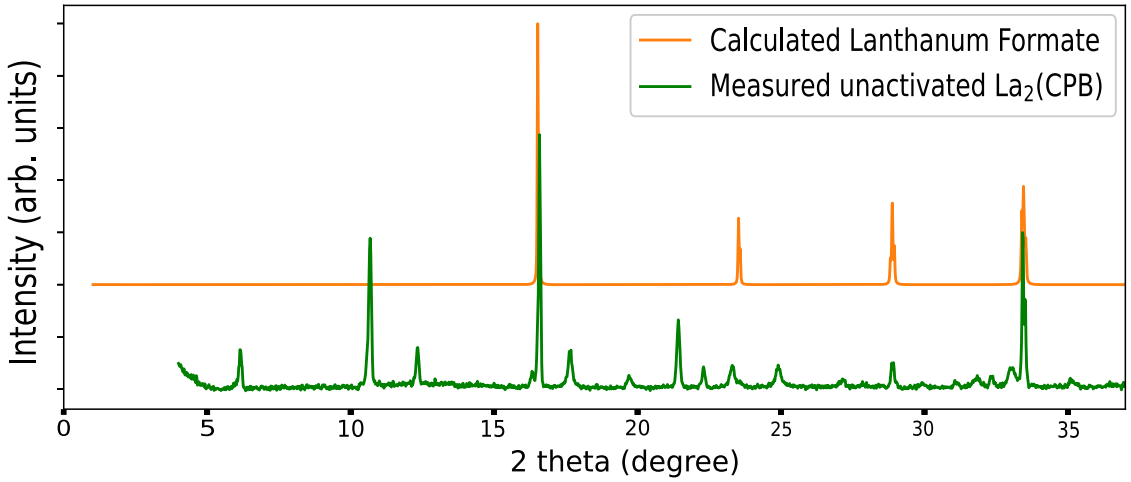

Figure 5.3: La_2(CPB) PXRD diffractogram in green compared with calculated Lanthanum formate diffractogram in red. The background signal in the La_2(CPB) diffractogram was subtracted.

By visually observing intensities of the peaks corresponding to La formate or Ce formate from plots like Figure 5.1, 5.2 and 5.3 for all batches, estimations of the weight percentage of impurity in the batches were made, see Table 5.1.

Table 5.1: Approximated impurity amounts and produced masses for each sample batch of La_2CPB and Ce_2CPB. The batches are named with La or Ce plus two numbers. The first number indicating synthesis occasion 1,2 or 3, and the second number indicating the batch number.

Sample batch.	Impurity mass percent per batch (%).	Produced mass (g).
La 1.1	0	0.15
La 1.2	< 30	0.15
La 2.1	10-30	0.153
La 2.2	< 30	0.177
La 2.3	< 30	0.169
La 3.1	10-30	0.469
Ce 1.1	10-30	0.15
Ce 1.2	< 30	0.15
Ce 1.3	< 30	0.15
Ce 2.1	< 30	0.1950
Ce 2.2	10-30	0.150
Ce 3.1	10-30	0.5

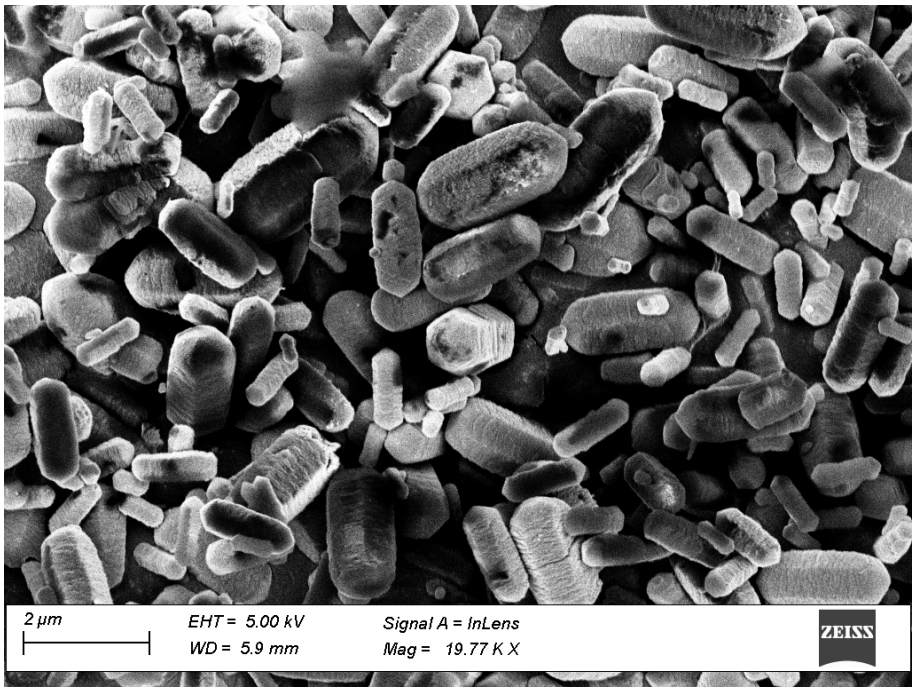

Figure 5.4: A SEM image of unactivated La_2(CPB).

Figure 5.4 shows rod shaped crystals with about 1 to 2 μm in length, and hexagonal shaped cross sections. The shape of the crystals matches the crystal structure that F.M. Amombo, L. Öhrström et al., derived in their study, as seen in Chapter 2.4.

5.2 Room temperature Raman spectroscopy

Figure 5.5, shows two spectra that were repeatedly measured for the total 10 (5+5) batches of La_2(CPB) and Ce_2(CPB). As seen the spectra are almost identical, which is expected because of the similarities in structure. No signs of band frequency shifts could be found related to the weight difference of La and Ce. Figure 5.6, shows two spectra of La_2(CPB), the orange colored is before activation when DMF was still in the pores, and the yellow is when it has been heated in 200 °C for 4h to remove the DMF and activate it. As seen the bands get burried in the background signal, and to get the spectrum without saturating the spectrometer of the Raman setup the instensity of the laser beam had to be lowered significantly. This is a strong indication of luminescence, that only occurred for the activated samples.

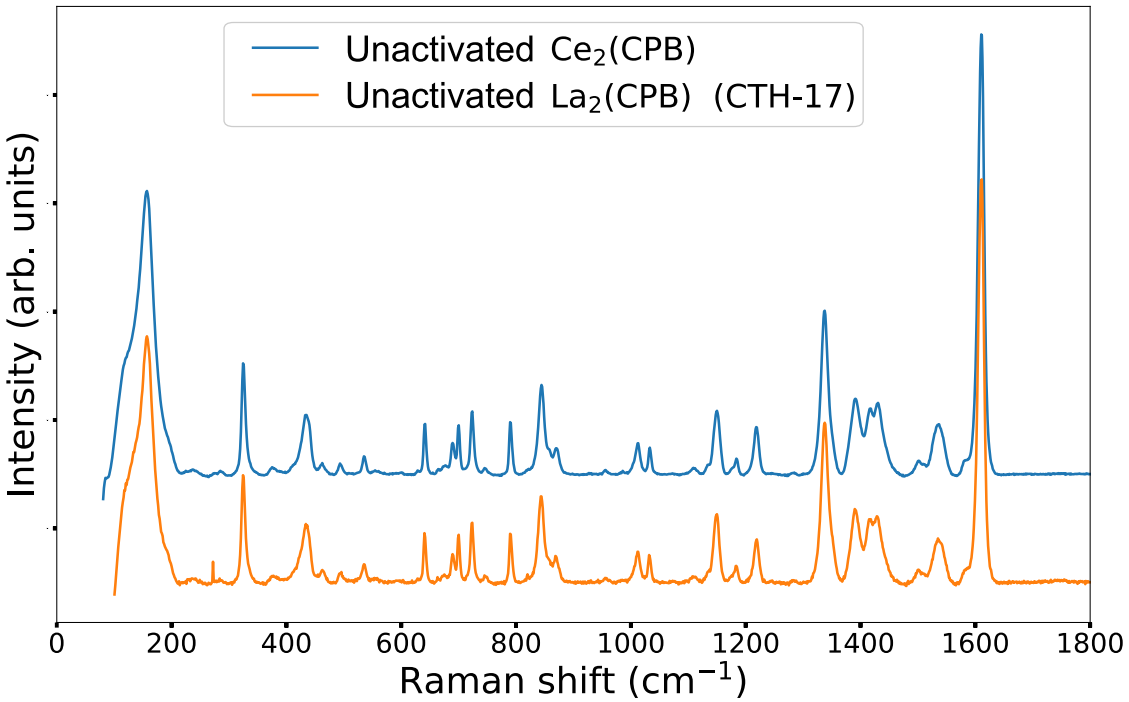

Figure 5.5: Raman spectra of unactivated La_2(CPB) in orange and unactivated Ce_2(CPB) in blue. Backgrounds have been subtracted in both spectra to make them flat. They were separated by a constant.

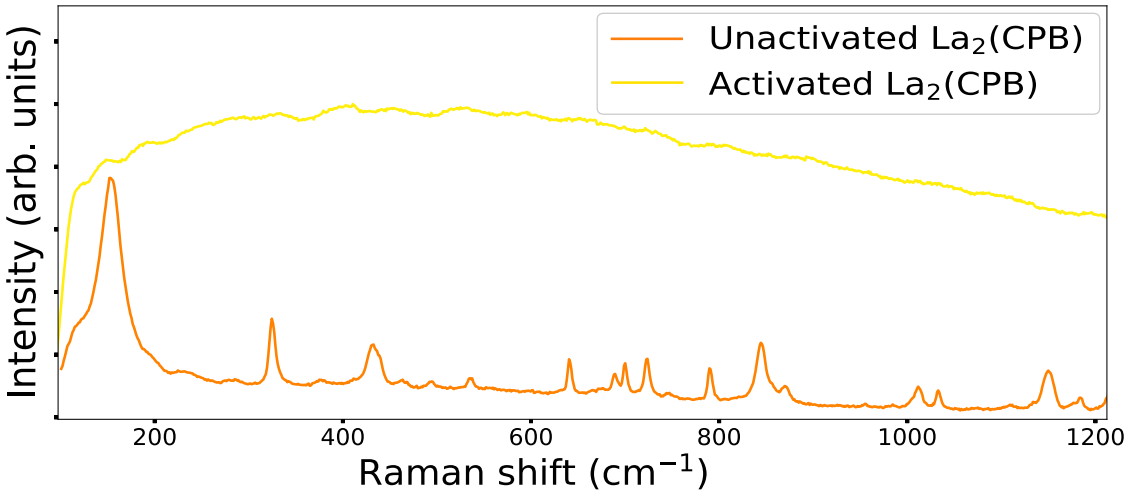

Figure 5.6: Raman spectra of La_2(CPB). One unactivated sample in orange, and one activated sample in yellow that was heated to 200 ° C under vacuum for 4 hours, and then left to cool down to room temperature before being measured.

5.2.1 Band assignments

To figure out which bands were from vibrations solely related to the MOFs, and which bands both occurring in the MOFs and in the linker spectrum, they were plotted together, see Figure 5.7. A spectrum of DMF was also plotted in the same figure since the MOFs were not activated before the measurements, which means that they still had DMF in the porous structure, as seen in Chapter 2.4. In Figure 5.7, most bands in the MOFs either occur in the spectrum of the CPB linker slightly shifted (green stars), or in the DMF spectrum (red stars). However, there are two small bands at 463 and 493 cm^{-1} that only occurs in the MOFs spectra, marked with two arrows to the left in Figure 5.7. Those could be related to the La-O and Ce-O bonds. It is assumed that La-O and Ce-O stretching vibrations are Raman active in the MOF structures even though they are bound to six oxygen atoms in a structural manner. This assumption will be supported later in the analysis of INS spectra. This assignment is further supported by a paper by H.N Abdelhamid et al., where the Raman spectrum of a similar MOF with La metal SBUs is investigated [26].

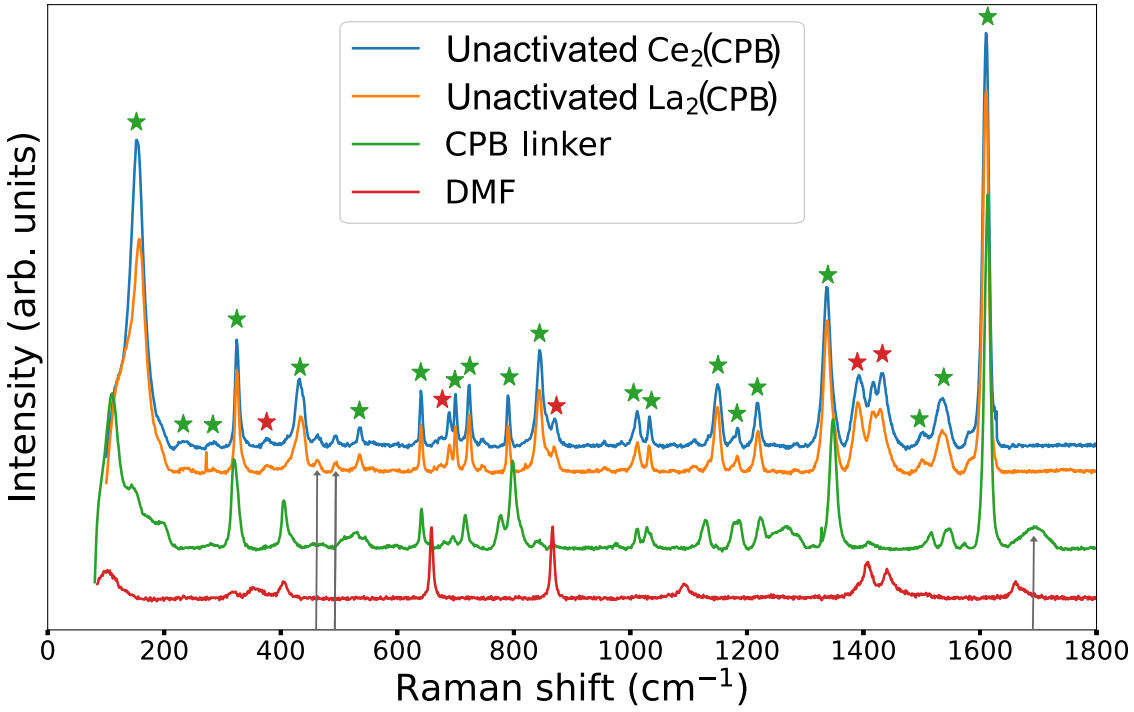

Figure 5.7: Raman spectra of unactivated La_2CPB, Ce_2CPB, the CPB-linker and DMF. The background was subtracted and the spectra were vertically separated with constants. Green stars indicate bands that are from the CPB-linker in the MOF structures, and red stars indicate bands that are from DMF.

They concluded that a band at 480 cm^{-1} in Infrared spectroscopy (IR) was from La-O stretching vibrations. The structure of that MOF is made up by a linker called 1.3.5-Tris(4-carboxyphenyl)benzene (BTB) which is similar to the CPB linker, but trigonal structured with three phenyl rings instead of the hexagonal CPB linker with six phenyl rings. A band with frequency close to 480 cm^{-1} from La-O and Ce-O vibrations could therefore potentially be visible in this spectra too.

There is also one band that occurs in the CPB linker spectrum but does not occur in the MOFs spectra, at 1694 cm^{-1}, pointed out with the arrow to the right in figure 5.7. The ends of the CPB-linker contains carboxyl groups (R-COOH), that later binds to lanthanum or cerium in the MOFs, and should therefore disappear in the MOF Raman spectra. Monomeric formic acid (HCOOH) has a stretching vibration of C=O at 1769 cm^{-1}, and at 1670 cm^{-1} in the dimeric form [38]. Possibly this is the vibration shown at 1694 in the CPB-linker spectrum, slightly shifted compared to formic acid, that disappear when lanthanum and cerium binds.

The rest of the bands in the MOFs should be from the CPB-linker which consists of carbon and hydrogen atoms in forms of connected aromatic rings. The strongest band of the MOFs and the linker at 1611 cm^{-1} seems to be from C=C stretching vibrations in the aromatic rings [39]. There are papers investing vibrations of similar MOFs, with the same CPB linker, or a similar linker, where they conclude that vibrations at 1580 and 1602 cm^{-1} that are from anti symmetrical vibrations of COO^- [38][40]. In the MOFs these vibrations are found in the carboxylate groups, and in the carboxyl group in the free CPB linker molecules when it is not coordinated to La or Ce. Perhaps this could be the relatively strong band at 1537 cm^{-1}. If this hypothesis is correct a frequency shift would be expected when the MOFs change in structure since the angle of the COO^- carboxylate group is suppose to change according to F.M. Amombo, L. Öhrström et al., and described in Chapter 2.4 [9].

There are plenty of reported studies in the literature investigating vibrational modes of benzene rings, but as mentioned in Chapter 3.1.2 the frequency of these vibrations will shift in the MOFs compared to a benzene molecule in free space, and additional types of vibrations might occur. Therefore these references can only be used as guidelines. Some interesting vibrations of benzene molecules are a_{1g} at 1276 cm^{-1}, e_{2g} at 1767, 1222 and 648 cm^{-1}, e_{1g} at 891 cm^{-1}, based on simulations reported in ref. [29]. Only the e_{2g} vibrations at 648 cm^{-1} and 1276 cm^{-1} seems to have some close related bands in the spectrum in Figur 5.7. Another paper shows a Raman spectra of a MOF made with a linker called 4,4-biphenyl dicarboxylate (bpdc), that has a C−C bonding connecting the phenyl rings, which shows a band at 1283 cm^{-1} [41]. Therefore the band at 1229 cm^{-1} in Figure 5.7 could potentially be the vibration of the C−C vibration for the part of the CPB linker that connects the phenyl ring to the two oxygen atoms, see Figure 3.4.

The second strongest band, most far to the left in the spectra with frequency 152 cm^{-1} in Figure 5.7 is within a low frequency region, and difficult to assign to any known vibration because of lack of published papers on low frequency vibrations of similar materials. The paper mentioned in Chapter 3.1 that investigates rotations of the linker units of a MOF called DUT-8, is the closest relevant paper that could be found [30]. They assign a band at 20 cm^{-1} as rotation of a linker with double aromathic rings when the structure is in closed phase, and at 60 cm^{-1} when its in open phase. The phenyl rings in La_2CPB and Ce_2CPB only consists of one aromathic ring, meaning that a libration or vibration of these would most probably have a higher frequency than a linker with double aromathic rings. With this reasoning the band at 152 cm^{-1} in Figure 5.7, could therefore potentially be from phenyl ring librations or rotations, and worth to further investigate with variable temperature measurements.

Table 5.2: Tentative band assignments from Raman spectra of La_2CPB and Ce_2CPB. Bands that could not be assigned are filled in with "-". The symbol v stands for vibration, v_{as} is anti symmetrical vibration, and v_s is symmetrical vibration.

Raman bands.	Vibrational modes.	References.
1611	v(C=C)	[39][41]
1537	$v_{as}(COO^-)$	[38] [40]
1434	DMF related	Fig 5.7
1418	DMF related	Fig 5.7
1395	DMF related	Fig 5.7
1337	-	-
1229	v(C−C)	[29] [41]
1184	-	-
1150	-	-
1035	-	-
1013	-	-
871	DMF related	Fig 5.7
844	-	-
790	-	-
723	-	-
700	-	-
690	DMF related	Fig 5.7
640	v(C−C)	[29]
537	-	-
495	v(La−O)/v(Ce−O) ?	[26] [40]
463	v(La−O)/v(Ce−O) ?	[26] [40]
434	-	-
376	DMF related	Fig 5.7
326	-	-
152	Phenyl ring libration or rotation ?	[30]

5.3 Variable temperature Raman spectroscopy

Figure 5.8, 5.9, 5.10 and 5.11 show Raman spectra of La_2(CPB) and Ce_2(CPB) when the temperature is varied betwen -100 °C and 350 °C. For both MOFs the spectrometer in the Raman setup got saturated when the sample temperature reached 400 °C, and also when new measurements were made on the same samples in room temperature. This means that after 400 °C some irreversible phase change of the materials had occurred.

5.3.1 DMF related bands

A spectrum of measured liquid DMF was placed in the same figure so that changes in the bands possibly related to DMF in the structures of the unactivated samples could be observed.

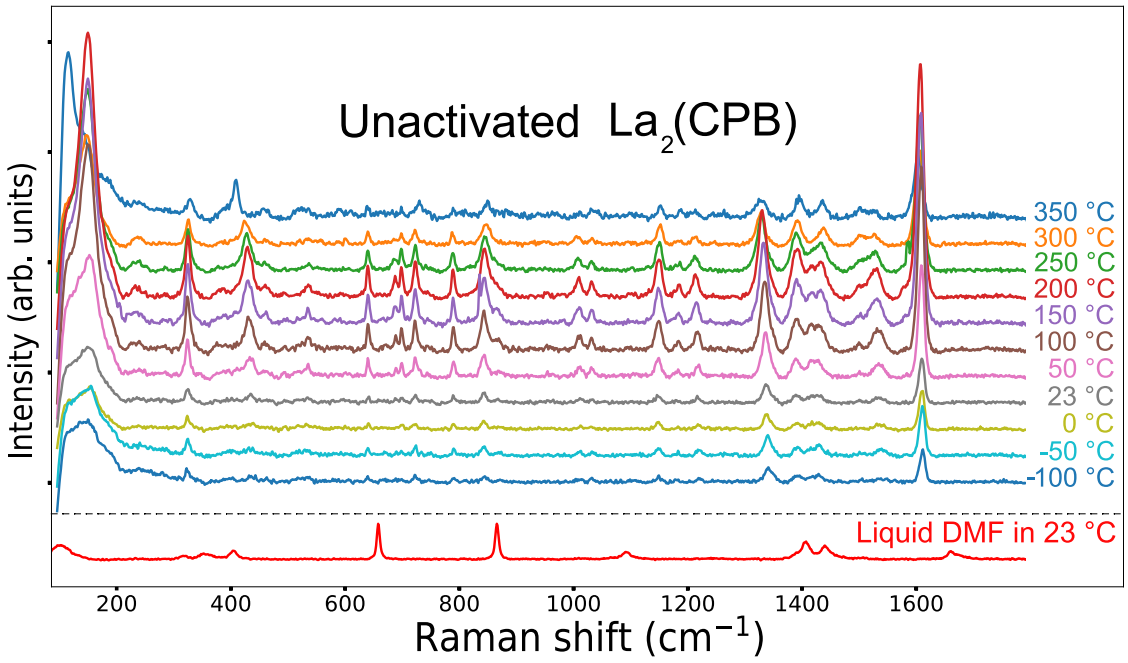

Figure 5.8: Temperature variational Raman spectra of unactivated La_2(CPB) in temperatures between -100 and 350 °C. Background signals have been subtracted, and the spectra are separated by added constants. The spectrum closest to the x-axis is from another measurement of DMF.

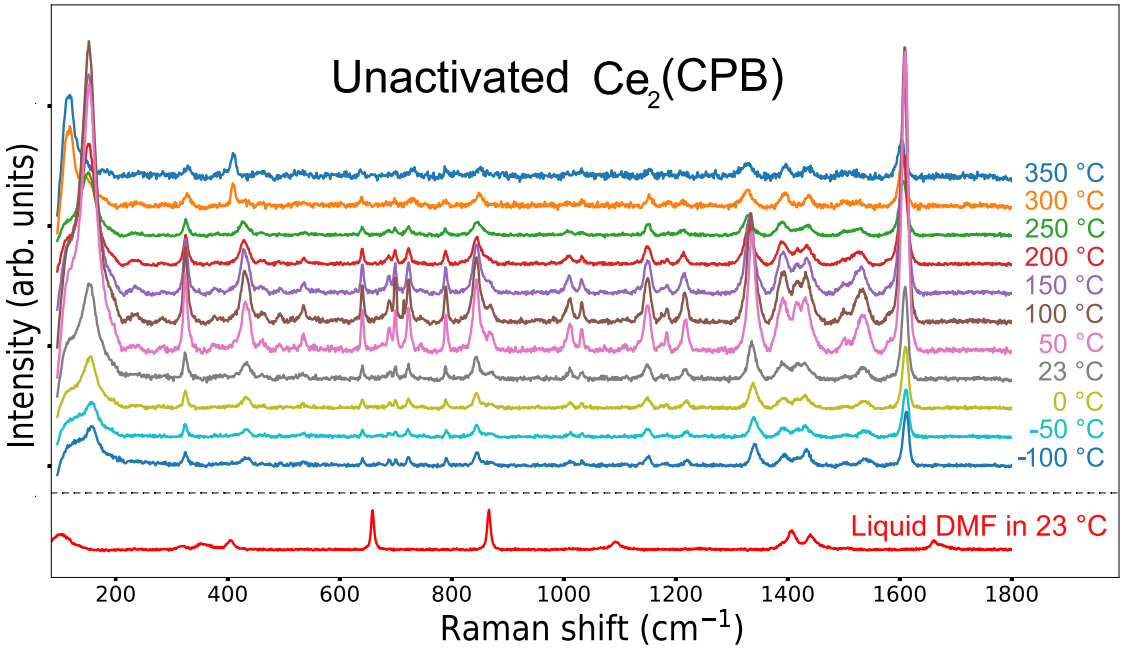

Figure 5.9: Temperature variational Raman spectra of unactivated Ce_2(CPB) in temperatures between -100 and 350 °C. Background signals have been subtracted, and the spectra are separated by added constants. The spectrum closest to the x-axis is from another measurement of DMF.

Notice what happens to the bands in the MOFs at 871 and 1418 cm^{-1} that were assigned as DMF related in the previous section. The intensity of those bands varies significantly with temperature. From temperature 50 °C and upwards the intensities of the bands are strong, but seems to disappear in relation to neighboring bands between 200 and 250 °C, or possibly combine with the neighboring bands. If those bands are related to the DMF it is a strong indication that DMF leaves the pores of the MOFs somewhere between those two temperatures, since that would mean that bonds get broken and the associated vibrational modes disrupt. The same thing seems to happen with Ce_2(CPB) sample. Although, it could also be that because of increased background luminescence with increased temperature as observed in Figure 5.6, the bands with lower intensity get drowned in the background luminescence signal and therefore seem to ”disappear”. If it is DMF leaving the pores, a reasonable question to ask is: does DMF leave the structure because of the opening of the structure (phenyl ring rotation and stretching in the rod direction) as described in chapter 2.4? In that case, some band peak shifts related to the tentative assignments of the La-O vibrations, phenyl ring libration or rotation, and COO^- anti symmetrical vibration is expected to happen. This is investigated in the next chapter. Also notice what happens after 300 °C in figure 5.8 and after 250 °C in figure 5.9, for the bands at 434 and 152 cm^{-1}. Those bands were not assigned as DMF related in Table 5.2, but they show a strong irreversible shift to lower frequencies which could be related to the observed irreversible increase in luminescence as mentioned in Section 5.3. This is also investigated in the next chapter.

5.3.2 Bands related to phenyl ring rotation and stretching of the MOF

In Figure 5.10 and 5.11 there are three zoomed in images of the spectra at the tentative locations of the phenyl ring libration or rotation band (a), the La-O/Ce-O vibration band (b), and the COO^- anti symmetrical vibration in the carboxylate group (c). The zoomed in spectra are stacked in order with increasing temperature (along the y-axis) by adding constants to the intensity.

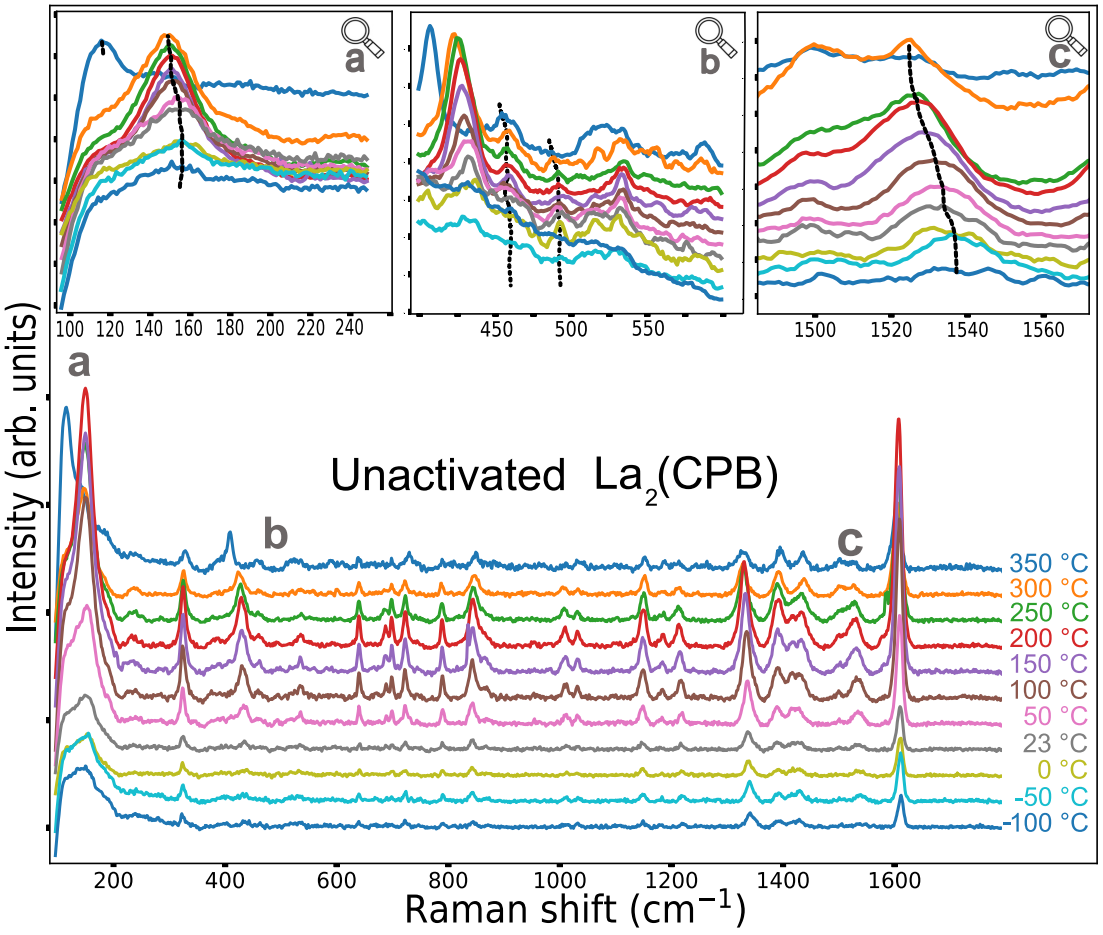

Figure 5.10: Temperature variational Raman spectra of La_2(CPB) with zoomed-in figures on location (a), (b), and (c). The spectra have their background subtracted, and they are separated with constants. The lines in panels (a-c) are guides to the eye to mark the temperature trend of the peak positions.

The dotted trend lines made by visual estimation show linear peak shifts between room temperature and 300 °C for the phenyl ring libration (a), and the COO^- stretching (c), which normally indicates thermal expansion [42]. No clear shifting trend for La-O or Ce-O vibrations was observed. F.M. Amombo, L. Öhrström et al., reported three different space groups, $P6_122$, $P622$, and $P6/mmm$, observed at temperatures 90 K, 300 K and 500 K (= -183.15°C, 23°C and 226.85°C). It is therefore likely that the first trend between -100 and 0°C where the bands are not shifting is when the structure is fixed in space group $P6_122$. After that a gradual change of the crystal structure from space group $P622$ to $P6/mmm$ happens, in combination with DMF leaving the pores, and the thermal expansion. Finally one last phase shift happens, that is the big peak shift between 300 and 350 °C for La_2(CPB) and between 250 and 300 °C for Ce_2(CPB), seen in zoom-in (a) and (b), in Figure 5.10 and 5.11. The fact that the strong shift happens after the indications of DMF leaving the porous structures of La_2(CPB) and Ce_2(CPB) could mean that the pores need to be free from molecules to undergo a phase change.

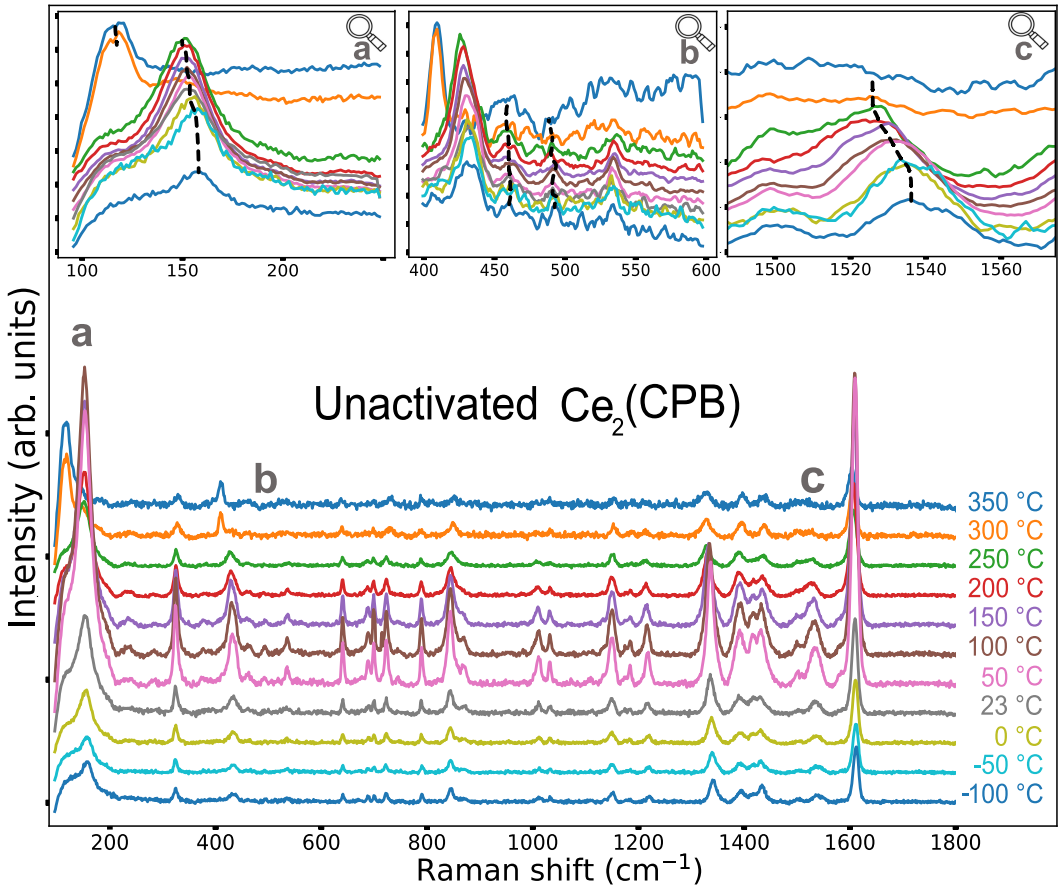

Figure 5.11: Temperature variational Raman spectra of Ce_2(CPB) with zoomed-in figures on location (a), (b), and (c). The spectra have their background subtracted, and they are separated with constants. The lines in panels (a-c) are guides to the eye to mark the temperature trend of the peak positions.

It also seems like there needs to be some thermal expansion in the structures before the strong shift can happen. Possibly this could be the stretching in the rod direction of La_2(CPB) and Ce_2(CPB), that needs to happen before the phenyl rings can twist, as described in Section 2.4. However, it is not clear what this strong phase shift is, since it happens for a much higher temperature than 500 K where the crystal structure belonging to space group $P6/mmm$ was found. It could be a new phase of the structure, or a first stage in a break down of the MOFs. It is an irreversible phase change since the spectra stayed the same after the change, when measured in lower temperatures down to room temperature. To check if the sample still contained a MOF after the unknown phase change, a new PXRD measurement was made on the La_2(CPB) sample i room temperature. See figure 5.12.

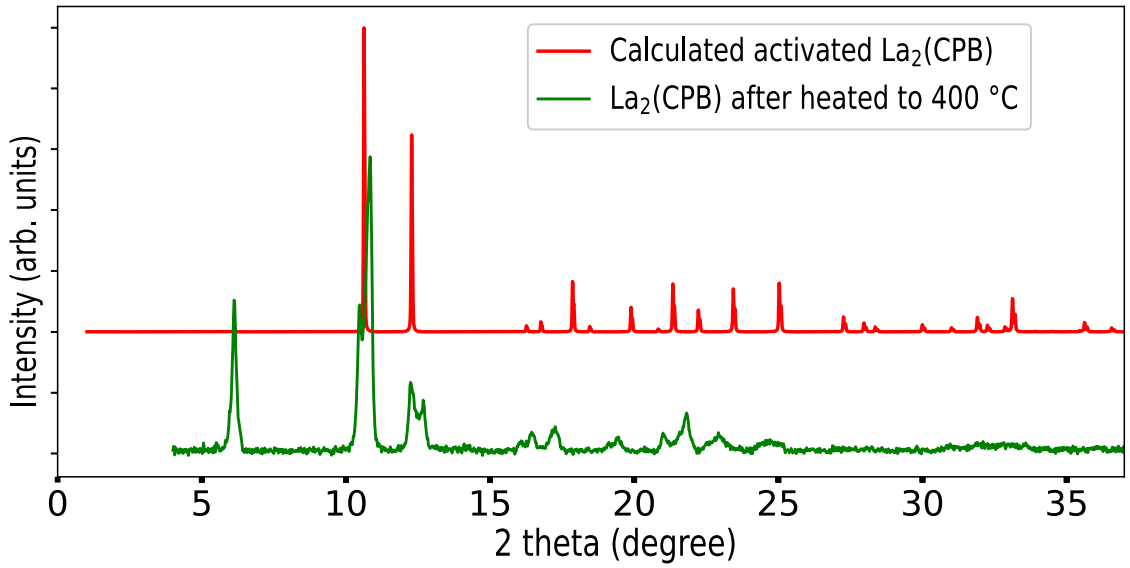

Figure 5.12: Calculated and measured PXRD diffractograms of La_2(CPB). The green measured diffractogram had the background subtracted to make it flat.

The measured diffractogram shows clear indications of a MOF when compared with the calculated diffractogram. The MOF has clearly changed in crystalline structure. New peaks can for instance be seen at around 11 and 13 degrees (2θ). This can also be seen in a temperature variational PXRD measurement of CTH-17 made by F.M. Amombo, L. Öhrström et al [9]. See Appendix A Figure A.4, to see those diffractograms.

5.4 Inelastic neutron scattering

Figure 5.13, shows the full INS spectra of activated samples of La_2(CPB) and Ce_2(CPB) measured at ISIS Neutron and Muon Source facility in Oxfordshire, the U.K. A first conclusion about the spectra is that they are very similar to each other, which indicates similar vibrational dynamics in the crystal structures. However they are not as similar to each other as in the Raman spectroscopy measurements. Some differences can be observed especially in the low energy region, 0-200 cm^{-1}, where the suggested bands of the vibrating phenyl ring is located. Overall, most of the bands are at the same locations, however some are hard to tell apart from noise, and some bands might come from La formate or Ce formate impurity. The fact that they are almost identical lowers the probability that some bands are from formate impurities, since that would most probably show up as a distinct difference in one of the spectra compared to the other, unless they have similar amounts of impurity. Unfortunately there were no time slots available at ISIS Neutron and Muon source for an additional measurement of La or Ce formate. Otherwise a spectrum of formate could have been used as reference spectrum to count out impurity bands.

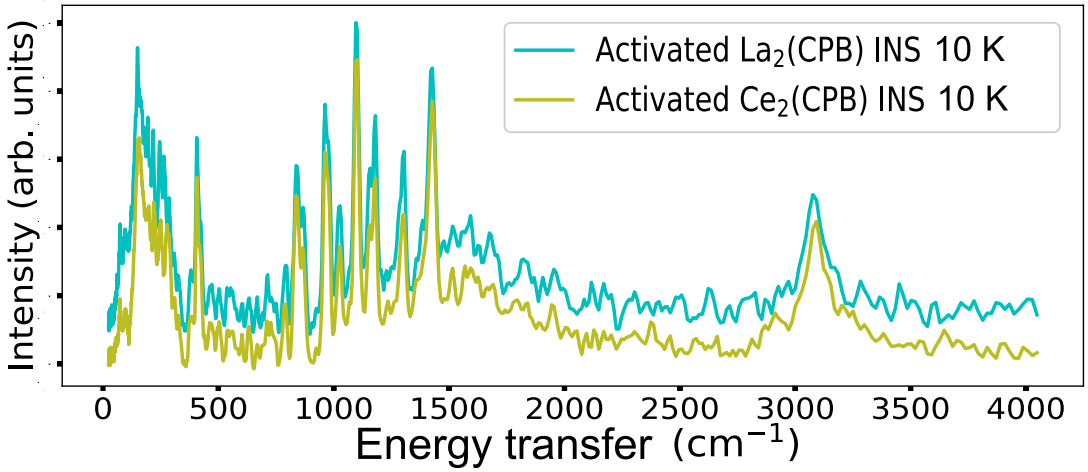

Figure 5.13: Full range INS spectra of activated La_2(CPB) and Ce_2(CPB), measured in temperature 10 K. Background signals have been subtracted, and the spectra are separated by added constants.

Figure 5.14, shows a comparison for La_2(CPB) and Ce_2(CPB) between Raman spectroscopy measurements, and INS measurements. As expected plenty of new bands shows up in the INS spectra since there are no selection rules, and all vibrations can scatter the neutrons as explained in Chapter 3.2. The intensities are also different, hydrogen has the largest cross-section valuse and scatter most, also explained in Chaper 3.2. With that knowledge it is of interest to look at the intensities of the tentative bands of phenyl ring librations or rotations at 152 cm^{-1}, La-O vibrations at 495 cm^{-1}, and COO^- anti symmetrical vibrations, all marked with arrows in the figure. As seen in Figure 5.14, the intensity of the band at 152 cm^{-1} is strong in relation to the other bands, indicating vibrations with hydrogen involved. This strengthen the hypothesis that the band is from phenyl ring librations, since they are comprised of a carbon and hydrogen complex (benzene ring with a COO^- functional group). The tentative bands of La-O/Ce-O, and COO^- vibrations are on the other hand low in intensity compared to the other bands. This also strengthen the hypothesis of the assignments of those bands.

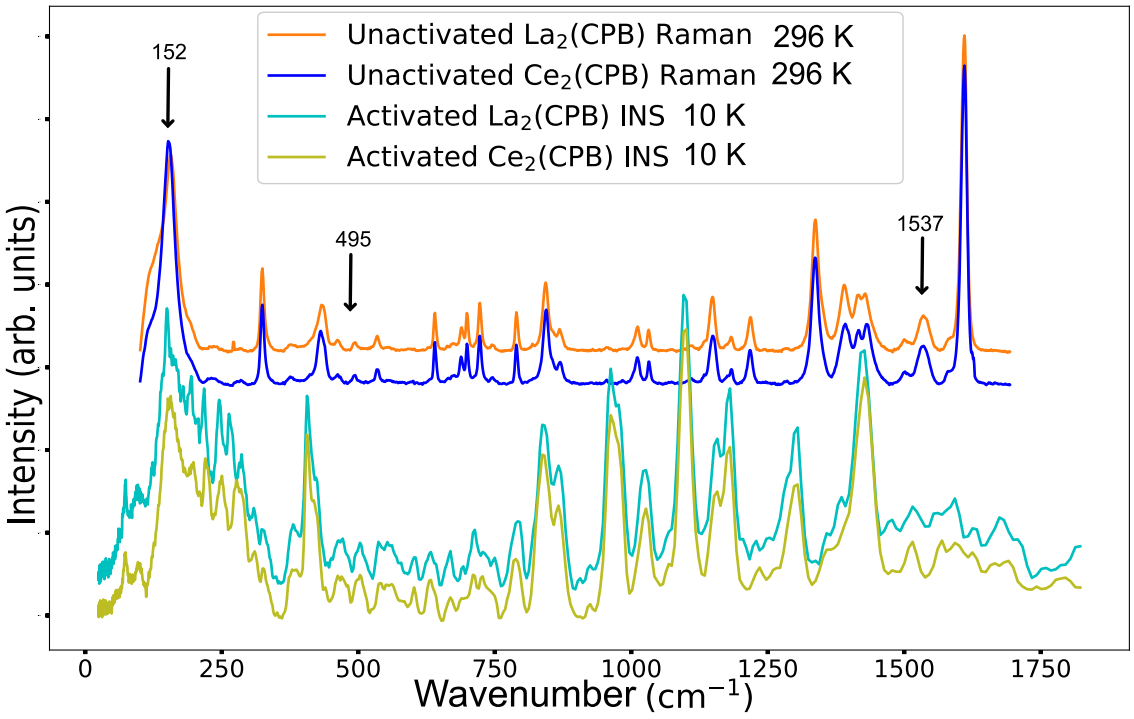

Figure 5.14: Raman spectroscopy measurements of unactivated La_2(CPB) and Ce_2(CPB) in orange and blue, compared to INS spectroscopy measurements of activated La_2(CPB) and Ce_2(CPB) in neon and olive green. The arrows indicate the positions of phenyl ring libration or rotation, La-O/Ce-O vibration and COO^- anti symmetrical vibration. Background signals have been subtracted, and the spectra are separated by added constants.

6
Conclusions

To conclude, the results of the thesis show

i Raman spectra of La_2(CPB) (CTH-17) and Ce_2(CPB) are virtually identical, suggesting that the type of metal cation (La or Ce) only has a minor effect on the local structure and vibrational dynamics of $\{La,Ce\}_2$(CPB).

ii Raman measurements of activated samples of La_2(CPB) and Ce_2(CPB) (heated to 200 °C under vacuum for 4h) show indications of photoluminescence when using a 785 nm laser.

iii Variable temperature Raman spectroscopy measurements of unactivated La_2-(CPB) and Ce_2(CPB) (with DMF trapped in the pores) indicate the release of DMF from the pores at around 200-250 °C.

iv Bands tentatively assigned to phenyl ring libration or vibration, and COO^- anti symmetrical vibrations in the carboxylate group show similar behaviour in shifting trends. First no shift in frequency between -100 to 0 °, then a linearly shifting trend in frequency with increased temperature indicating thermal expansions.

v No frequency shifts in any temperatures (-100 to 400 °C) can be observed for the tentatively assigned band of La-O/Ce-O vibrations for La_2(CPB) and Ce_2(CPB). This indicate that this vibration is not affected by a crystal structure change in the material.

vi An irreversible phase change of the spectra is observed in the temperature interval 300 to 350 °C for La_2(CPB) and 250 to 300 °C for Ce_2(CPB), indicating a new unknown phase of the crystal structures. This structure shows photoluminescence, both in temperature 400 °C and in room temperature.

vii INS spectra of La_2(CPB) (CTH-17) and Ce_2(CPB) are also virtually identical, which further strengthens the proposed conclusion in (i).

7
Perspectives

For the purpose of investigating local structure and dynamics of La_2(CPB) and Ce_2(CPB), it would be beneficial to find a synthesis method that does not produce any formate byproduct. The observed luminescent properties of these MOFs would be interesting to further investigate. Perhaps it could be used for sensing technologies since it seems like the luminescence activates when the pores get empty. Would it behave the same if there was other particles in the pores, such as CO_2? To further investigate the vibrational properties of these MOFs it would be interesting to do DFT calculations, and possibly simulate Raman spectra and INS spectra to compare with the measured results in this study. It would also be interesting to do variable temperature IR (and of course INS if possible) measurements to compare with Raman, and to be able to analyse more (or all) vibrational modes in different temperatures. It would also be interesting to do SCXRD measurements in room temperature of both MOFs after being heated to 400 ° to see if any new structure can be assigned that would explain the big frequency shift observed in the variable temperature Raman spectroscopy measurements. Also to do SEM measurements after being heated to see if the crystals look different when DMF is out of the pores, and ones there is a potentially new phase of the crystal structure.

Bibliography

[1] Francoise M. Amombo Noa, Lars Öhrström, *Metal-Organic Frameworks*. American Chemical Society, March 25 2021, ch. MOFs versus Other Currently Commercially Used Porous Materials. DOI: 10.1021/acs.infocus.7e4004.

[2] Yi Peng et al., "Metal-organic framework (mof) composites as promising materials for energy storage applications," *Advances in Colloid and Interface Science*, vol. 307, 2022, ISSN: 0001-8686. DOI: 10.1016/j.cis.2022.102732.

[3] Hannelore Konnerth et al., "Metal-organic framework (mof)-derived catalysts for fine chemical production," *Coordination Chemistry Reviews*, vol. 416, 2020, ISSN: 0010-8545. DOI: 10.1016/j.ccr.2020.213319.

[4] Qihui Qian et al., "Mof-based membranes for gas separations," *Chemical Reviews*, vol. 120, no. 16, 2020, ISSN: 8161-8266. DOI: 10.1021/acs.chemrev.0c00119.

[5] Omar M. Yaghi et al., "Water adsorption in porous metalorganic frameworks and related materials," *American Chemical Society*, vol. 136, no. 11, 2014, ISSN: 8161-8266. DOI: 10.1021/ja500330a.

[6] Jie Liang et al., "A robust aluminum metal-organic framework with temperature-induced breathing effect," *ACS Materials Letters*, vol. 2, no. 3, 2020. DOI: 10.1021/acsmaterialslett.9b00399.

[7] Caroline Mellot-Draznieks et al., "Very large swelling in hybrid frameworks: A combined computational and powder diffraction study," *Journal of the American Chemical Society*, vol. 127, no. 46, 2005, ISSN: 16273-16278. DOI: 10.1021/ja054900x.

[8] Andreas Schneemann et al., "Flexible metalorganic frameworks," *Chemical Society Reviews*, vol. 43, 2014. DOI: 10.1039/C4CS00101J.

[9] Francoise M. Amombo Noa, Lars Öhrström et al., "Chiral lanthanum metalorganic framework with gated co2 sorption and concerted framework flexibility," *Journal of the American Chemical Society*, vol. 144, no. 19, 2022. DOI: 10.1021/jacs.2c02351.

[10] Francoise M. Amombo Noa, Lars Öhrström, *Metal-Organic Frameworks*, 1st ed. American Chemical Society, March 25 2021, ch. The Chemistry of MOF. DOI: 10.1021/acs.infocus.7e4004.

[11] Omar M. Yaghi et al., "Design and synthesis of an exceptionally stable and highly porous metal-organic framework," *Nature*, vol. 402, 1999. DOI: 10.1038/46248.

[12] Omar M. Yaghi et al., "Hydrogen storage in microporous metal-organic frameworks," *Science*, vol. 300, 2003. DOI: 10.1126/science.1083440.

[13] Kranthi Kumar Ganguab, Suresh Maddila and Sreekantha B. Jonnalagadda, "The pioneering role of metalorganic framework-5 in ever-growing contemporary applications a review," *Royal society of chemistry*, vol. 12, 2022. DOI: 10.1039/D2RA01505F.

[14] Manel Bergaoui et al., "A review of the features and applications of zif-8 and its derivatives for separating co2 and isomers of c3- and c4- hydrocarbons," *Journal of Natural Gas Science and Engineering*, vol. 96, 2021. DOI: 10.1016/j.jngse.2021.104289.

[15] Steven S. Kaye et al., "Impact of preparation and handling on the hydrogen storage properties of zn4o(1,4-benzenedicarboxylate)3 (mof-5)," *American Chemical Society*, vol. 129, pp. 14 106–14 528, 46 2007. DOI: 10.1021/ja076877g.

[16] Nobuo Hara, *Encyclopedia of Membranes*, 1st ed. Springer-Verlag Berlin Heidelberg, 2016, ch. ZIF-8 Membrane, pp. 2064–2067. DOI: 10.1007/978-3-662-44324-8_1988.

[17] Francoise M. Amombo Noa, Lars Öhrström, *Metal-Organic Frameworks*, 1st ed. American Chemical Society, March 25 2021, ch. Reticular chemistry. DOI: 10.1021/acs.infocus.7e4004.

[18] Cambridge Crystallographic Data Centre (CCDC). "Access structures." (2022), [Online]. Available: https://www.ccdc.cam.ac.uk/structures/ (visited on 05/2024).

[19] K. Momma and F. Izumi, "Vesta 3 for three-dimensional visualization of crystal, volumetric and morphology data," *Journal of Applied Crystallography*, vol. 44, 2011. DOI: 10.1107/S0021889811038970.

[20] Susumu Kitagawa, Ryo Kitaura, Shin-ichiro Noro, "Functional porous coordination polymers," *Angewandte Chemie International Edition*, vol. 43, no. 18, 2004. DOI: 10.1002/anie.200300610.

[21] Shi-Yuan Zhang et al., "Modulation of water vapor sorption by a fourth-generation metalorganic material with a rigid framework and self-switching pores," *Journal of the American Chemical Society*, vol. 140, no. 39, 2018. DOI: 10.1021/jacs.8b07290.

[22] Eugeny V. Alexandrov et al., "Topological transformations in metalorganic frameworks: A prospective design route?" *CrystEngComm*, vol. 24, 2022. DOI: 10.1039/D2CE00264G.

[23] François-Xavier Coudert et al., "Topological transformations in metalorganic frameworks: A prospective design route?" *The Journal of Physical Chemistry Letters*, vol. 4, no. 19, 2013. DOI: 10.1021/jz4013849.

[24] Paul H. L. Walter et al., *C.V. Raman and the Raman Effect - International Historic Chemical Landmark*, 1st ed. American Chemical Society, December 15 1998.

[25] Marek Prochazka, *Surface-Enhanced Raman Spectroscopy*, 1st ed. Springer Cham, 2016, ch. Basics of Raman Scattering (RS) Spectroscopy, pp. 7–19. DOI: 10.1007/978-3-319-23992-7_2.

[26] Hani Nasser Abdelhamid et al., "Luminescence properties of a family of lanthanide metal-organic frameworks," *Microporous and Mesoporous Materials*, vol. 279, 2019. DOI: 10.1016/j.micromeso.2019.01.024.

[27] Richard Allen Nyquist, *Interpreting Infrared, Raman, and Nuclear Magnetic Resonance Spectra*, 2nd ed. Academic Press, 2002, ch. Benzene and Its Derivatives, pp. 351–423. DOI: 10.1016/B978-012523475-7/50189-3.

[28] Shaoqing Wang, "Intrinsic molecular vibration and rigorous vibrational assignment of benzene by first-principles molecular dynamics," *Scientific Reports*, vol. 10, 2020. DOI: 10.1038/s41598-020-74872-6.

[29] John J. Nash, "Benzene, c6h6 (d6h)," 10-11-2013. [Online]. Available: https://www.chem.purdue.edu/jmol/vibs/c6h6.html (visited on 05/12/2024).

[30] Alexander E. J. Hoffman, "The role of phonons in switchable mofs: A model material perspective," *Journal of Materials Chemistry A*, vol. 11, no. 28, 2023. DOI: 10.1039/D3TA02214E.

[31] Zhonglin Li et al., "Temperature-dependent raman spectroscopy studies of 15-layer wse2," *Nano Research*, vol. 13, 2020. DOI: 10.1007/s12274-020-2669-0.

[32] Philip C H Mitchell et al., *Vibrational SPectroscopy with Neutrons*. World Scientific Publishing, 2005, vol. 3. DOI: 10.1142/5628.

[33] Team TOSCA, "Tosca user manual," [Online]. Available: https://www.isis.stfc.ac.uk/Pages/tosca-user-manual6685.pdf (visited on 05/2024).

[34] Bruker, "D8 discover," 2024. [Online]. Available: https://www.bruker.com/en/products-and-solutions/diffractometers-and-x-ray-microscopes/x-ray-diffractometers/d8-discover-family/d8-discover.html (visited on 05/2024).

[35] Chalmers, "Sem: Leo ultra," [Online]. Available: https://www.chalmers.se/en/infrastructure/cmal/instruments/electron-microscopy/sem-leo-ultra/ (visited on 05/2024).

[36] Renishaw, "Invia confocal raman microscope," [Online]. Available: https://www.renishaw.com/en/invia-confocal-raman-microscope--6260 (visited on 05/2024).

[37] Linkam, "Thms600," [Online]. Available: https://www.linkam.co.uk/thms600 (visited on 05/2024).

[38] Konstantin I. Hadjiivanov et al., "Power of infrared and raman spectroscopies to characterize metal-organic frameworks and investigate their interaction with guest molecules," *Chemical Reviews*, vol. 121, pp. 1286–1424, 3 2021. DOI: 10.1021/acs.chemrev.0c00487.

[39] J Tim Bulmer et al., "Uv raman spectroscopy of hydrocarbons," *The Royal Society*, 2004. DOI: 10.1098/rsta.2004.1449.

[40] Van-Dung Le et al., "A copper-functionalized zirconium metalorganic framework for catalytic oxidative carboxylation of olefins and co2," *New Journal of Chemistry*, vol. 48, pp. 5300–5310, 2024. DOI: 10.1039/D4NJ00076E.

[41] Nour Nijem et al., "Understanding the preferential adsorption of co2 over n2 in a flexible metalorganic framework," *American Chemical Society*, vol. 133, no. 32, 2011. DOI: 10.1021/ja2051149.

[42] Nianbei Li and Junjie Liu, "Accessing general relations for temperature coefficients of raman shifts in 2d materials," *Journal of Physics: Condensed Matter*, vol. 32, no. 28, 2020. DOI: 10.1088/1361-648X/ab7f07.

A

Appendix

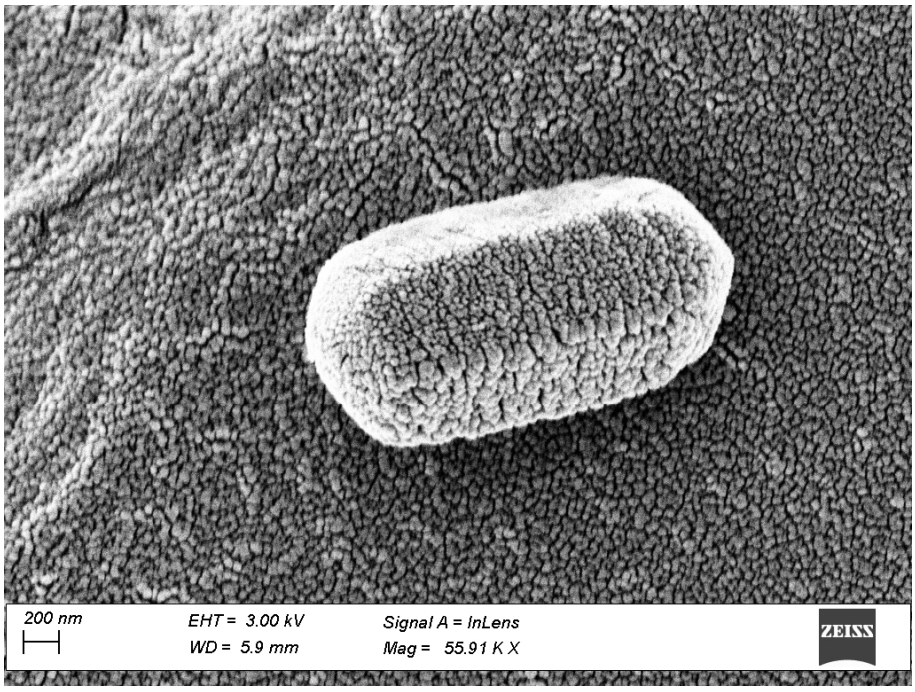

Figure A.1: A SEM image of unactivated La_2(CPB).

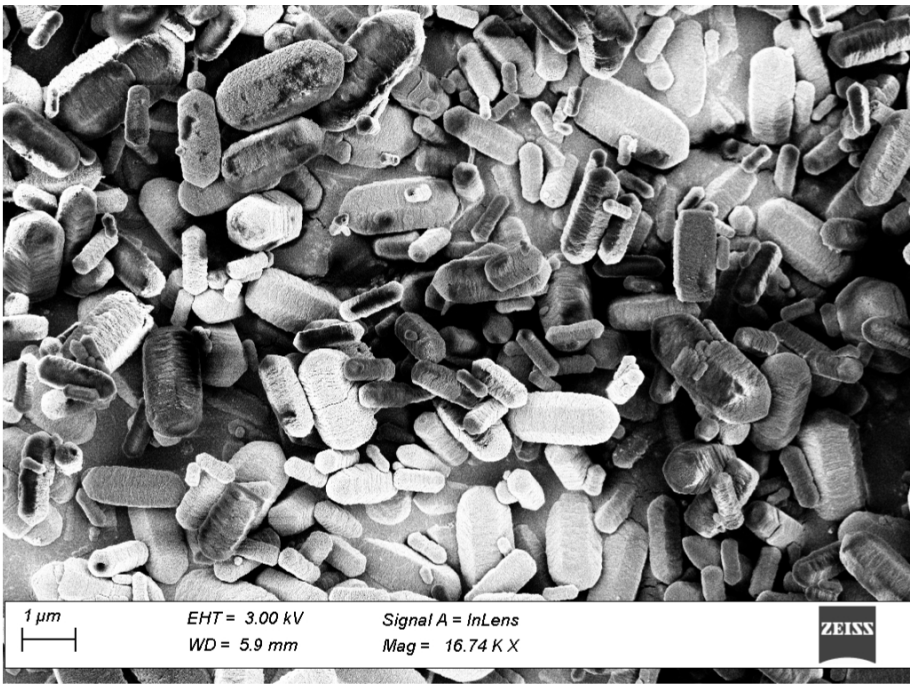

Figure A.2: A SEM image of unactivated La_2(CPB).

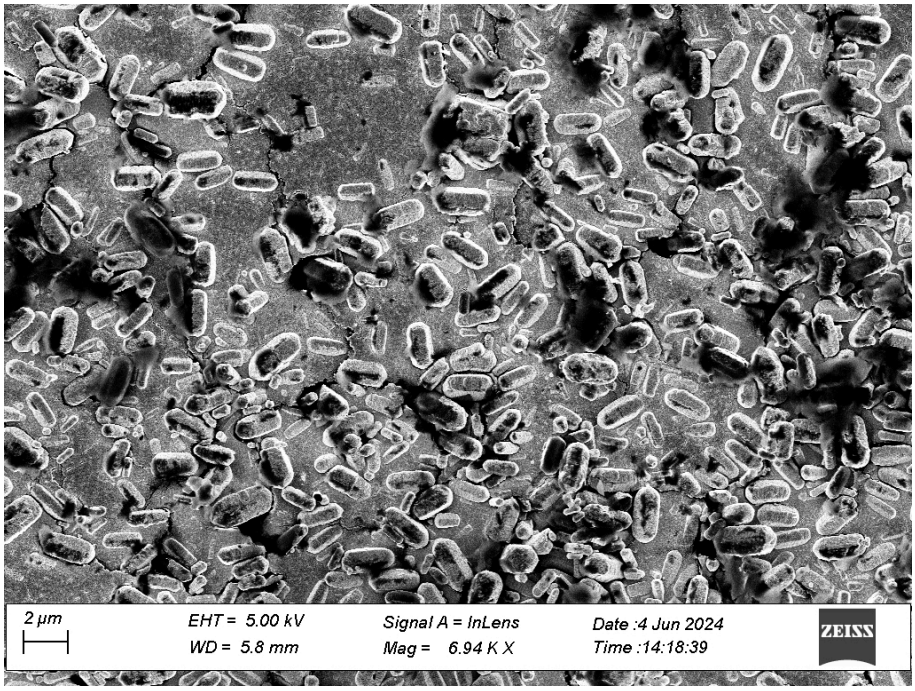

Figure A.3: A SEM image of unactivated La_2(CPB).

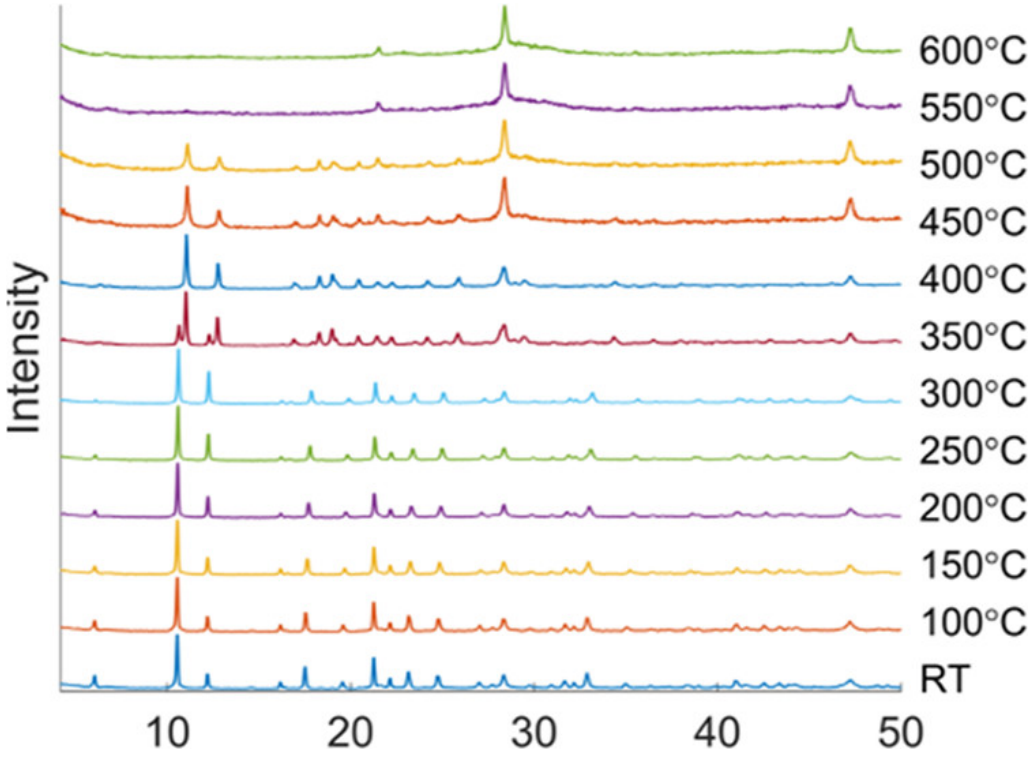

Figure A.4: Variable temperature PXRD of CTH-17 [La2(cpb)] · 1.5 DMF. The figure is reproduced with permission from ref. [9], Copyright (2022) American Chemical Society.

DEPARTMENT OF CHEMISTRY AND CHEMICAL ENGINEERING
CHALMERS UNIVERSITY OF TECHNOLOGY
Gothenburg, Sweden
www.chalmers.se

CHALMERS
UNIVERSITY OF TECHNOLOGY